A New Instrument for Time Resolved Measurement of HO_2 Radicals

Thomas H. Speak[1], Mark A. Blitz[1,2]*, Daniel Stone[1] and Paul W. Seakins[1,2]*

1 – School of Chemistry, University of Leeds, Leeds, LS2 9JT, UK

2 – National Centre for Atmospheric Science, Leeds, LS2 9JT, UK

Abstract

OH and HO_2 radicals are closely coupled in the atmospheric oxidation and combustion of volatile organic compounds (VOCs). Simultaneous measurement of HO_2 yields and OH kinetics can provide the ability to assign site specific rate coefficients that are important for understanding the oxidation mechanisms of VOCs. By coupling a FAGE LIF detection system for OH and HO_2 with a high pressure laser flash photolysis system, it is possible to accurately measure OH pseudo-first-order loss processes up to ~100000 s^{-1} and to determine HO_2 yields via time resolved measurements. This time resolution allows discrimination between primary HO_2 from the target reaction and secondary production from side reactions. The apparatus was characterized by measuring yields from the reactions of OH with H_2O_2 (1:1 link between OH and HO_2), with C_2H_4/O_2 (where secondary chemistry can generate HO_2), with C_2H_6/O_2 (where there should be zero HO_2 yield) and with CH_3OH/O_2 (where there is a well-defined HO_2 yield).

As an application of the new instrument, the reaction of OH with n-butanol has been studied at 293 and 616 K. The bimolecular rate coefficient at 293 K, $(9.24 \pm 0.21) \times 10^{-12}$ cm^3 $molecule^{-1}$ s^{-1}, is in good agreement with recent literature, verifying that this instrument can ~~both~~ measure ~~HO_2 yields and~~ accurate OH kinetics. At 616 K the regeneration of OH in the absence of O_2, from the decomposition of the β-hydroxy radical, was observed, which allowed the determination of the fraction of OH reacting at the β site (0.23 ± 0.04). Direct observation of the HO_2 product in the presence of oxygen has allowed the assignment of the α-branching fractions (0.57 ± 0.06) at 293 K and (0.54 ± 0.04) at 616 K), again in good agreement with recent literature; branching ratios are key to modelling the ignition delay times of this potential 'drop-in' biofuel.

1 Introduction

In the atmosphere, HO_2 and OH radicals (OH + HO_2 = HOx) are closely coupled via several reactions as shown in Scheme 1. The short lifetimes of HOx radicals mean that concentrations are determined by chemical production and removal and not by transport processes, making them ideal candidates as test species for our understanding of atmospheric chemical mechanisms (Stone et al., 2012;Monks, 2005;Stockwell et al., 2012).

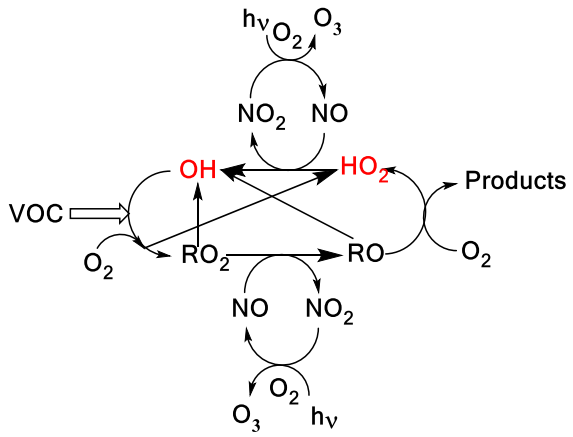

Scheme 1. A simplified tropospheric HOx cycle showing the importance of these short-lived radical species both to the chemical removal of VOCs and the formation of ozone.

In Scheme 1, the reaction of alkoxy radicals with molecular oxygen is a major route to HO_2 formation; however, this is not the only significant HO_2 formation process; for example, in the atmospheric oxidation of n-butanol, HO_2 can be formed via two different mechanisms. Abstraction by OH at the α position leads to a radical which reacts with oxygen to directly produce HO_2 (R1a, R2) whereas abstraction at other sites leads to alkylperoxy radical ($C_4H_9O_2$) formation with varying fractions of the RO_2 forming alkoxy radicals, and subsequently HO_2 (McGillen et al., 2013) on a longer timescale, see Scheme 2.

$$OH + CH_3CH_2CH_2CH_2OH \rightarrow CH_3CH_2CH_2CHOH + H_2O \quad \text{(R1a)}$$

$$CH_3CH_2CH_2CHOH + O_2 \rightarrow HO_2 + CH_3CH_2CH_2CHO \quad \text{(R2)}$$

The fraction of alkoxy radicals formed depends on the mechanism of RO_2 removal (reaction with NO or self or cross-reactions) and the yield of HO_2 from the alkoxy radical depends on the competition between decomposition, isomerization and reaction with O_2, which in turn will depend on the structure of the alkoxy radical, temperature, pressure and concentration of oxygen (Orlando et al., 2003). Therefore, in order to determine the HO_2 yield from the OH initiated oxidation of compounds such as n-butanol, it is important to have a selective, sensitive and time resolved method of HO_2 detection.

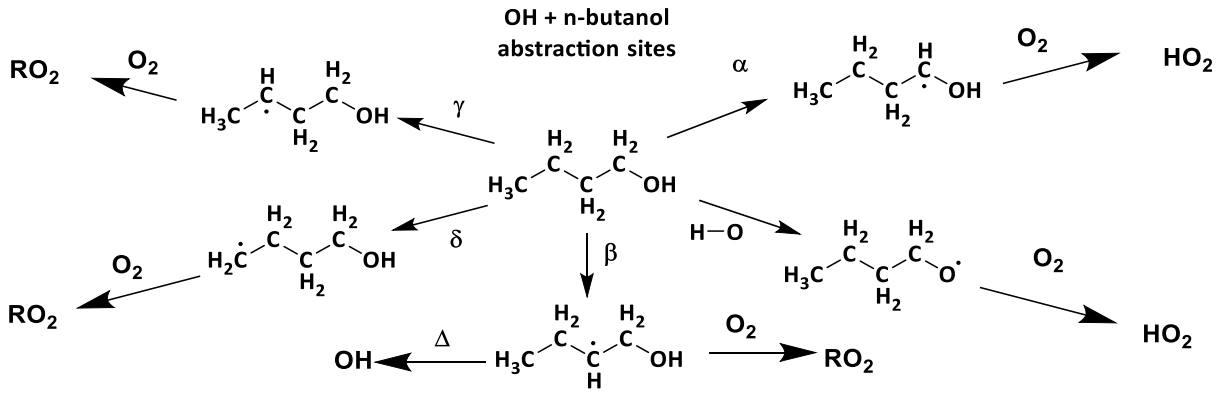

Scheme 2. The potential sites for OH abstractions in the oxidation of n-butanol. Of particular importance to low temperature combustion is the ratio of α to β branching fractions where α attack leads to chain inhibition and beta to chain propagation.

The importance of HO_2 chemistry is not limited to atmospheric processes; HO_2 is a key intermediate in low temperature (500 – 1000 K) combustion processes, particularly those involving oxygenated fuels (Zador et al., 2011). The mechanisms of low temperature combustion are of particular interest in the development of new engine technologies such as reactively controlled compression ignition (RCCI) (Reitz and Duraisamy, 2015) and are closely linked to atmospheric oxidation mechanisms. Monitoring HO_2 concentrations under the elevated temperatures and high pressures of combustion processes is therefore also of interest. In low-temperature combustion, HO_2 formation is a chain inhibition process, with OH reformation a chain propagating or chain branching process. The ratio of chain branching to chain inhibition processes is often the controlling factor in modelling ignition delay times (Agbro et al., 2017). High temperatures and concentrations of oxygen may be required to convert atmospheric processes, which take several 10s of seconds at ambient temperatures (and hence may be influenced by surface chemistry or secondary reactions) to the milli- or microsecond timescale where they can be studied by flash photolysis techniques without such interferences (Medeiros et al., 2018).

Direct measurements of HO_2 rely on absorption techniques, and kinetic information on HO_2 reactions has been determined mainly using absorption spectroscopy. This can be achieved either with conventional absorption techniques, often in the UV, (including multipass optics to enhance the pathlength) or in the IR with cavity ring down spectroscopy (CRDS) (Assaf et al., 2018;Onel et al., 2017). However, the HO_2 UV absorption spectrum (200 - 260 nm) is broad and

featureless (Crowley et al., 1991), and as such, overlaps with the UV absorptions of many other species present in atmospheric degradation pathways or combustion systems (particularly H_2O_2 and RO_2). To utilize the selectivity of the structured IR spectra, absorption methods have been developed in both the mid and near-IR (NIR) (Taatjes and Oh, 1997). Mid-IR absorption features for HO_2 provide sufficient absorption cross-sections for study (Jemialade and Thrush, 1990) but suffer from severe pressure broadening, reducing sensitivity under the conditions relevant to atmospheric and combustion systems (Thiebaud and Fittschen, 2006). Detection in the NIR has similar advantages in terms of a structured spectrum providing greater selectivity; the weaker absorption cross-sections are compensated by the higher powers and ease of use of NIR laser sources (Gianella et al., 2016). However, pressure broadening and interference from H_2O absorptions can make these measurements difficult at even low concentrations of water (10^{14} molecule cm^{-3}).

In the atmosphere (Stone et al., 2012) and in chamber studies (Glowacki et al., 2007), HO_2 is detected using a sensitive, but indirect method via conversion to OH, with detection of OH via laser induced fluorescence (LIF) (Hard et al., 1984;Brune et al., 1995;Fuchs et al., 2011) or conversion to $H_2{}^{34}SO_4$ with subsequent detection of the acid via mass spectrometry (Edwards et al., 2003;Hanke et al., 2002). In the LIF method, also known as Fluorescence Assay by Gaseous Expansion (FAGE (Hard et al., 1984)), which is the technique used in this study, OH is sampled into a low pressure region through a pinhole. Low pressures allow for the temporal separation of resonant 308 nm fluorescence from the excitation pulse. Following the first detection axis for OH, a flow of NO is introduced which reacts with HO_2 (R3):

$$HO_2 + NO \rightarrow OH + NO_2 \qquad \text{(R3)}$$

The resulting OH is monitored at a second detector. The high sensitivity with which OH can be detected gives HO_2 detection limits in the 10^8 molecule cm^{-3} range for 5 – 10 s averaging, however, to extract concentrations, both OH detection methods require calibration (Winiberg et al., 2015). For chamber measurements of HO_2, comparisons with direct CRDS measurements have verified the reliability of the calibration process (Onel et al., 2017).

HO_2 detection by LIF can be potentially sensitive to interferences from certain RO_2 species which may also be converted to OH on short timescales. Interferences can be minimized by short conversion times between NO injection and OH monitoring, utilizing low pressures, high flow

rates of the sample gas, and low NO concentrations to separate OH generation from HO_2 and RO_2, reduced conversion of HO_2 reduces the sensitivity of this technique and as such in practice a compromise between selectivity and sensitivity is used (Fuchs et al., 2011;Hard et al., 1984;Whalley et al., 2013).

The current paper describes a significant development on our earlier FAGE based instrument for time-resolved OH detection (Stone et al., 2016). In this improved system, laser flash photolysis in a high pressure (up to 5 bar), temperature controllable (300 – 800 K) reactor (shown in Figure 1) generated radicals which were then sampled through a pinhole forming a jet within the low pressure detection region (shown in more detail in Figure 2). OH radicals were monitored by LIF close to the pinhole. The jet breaks down after ~20 mm and NO was injected after this point to convert some HO_2 into OH which was then detected by a second monitoring system. In general, LIF becomes less sensitive at higher temperatures (due to distribution of population over more rotational levels) and O_2 concentrations (due to quenching). Sampling into the low-pressure region reduces both the effect of collisional quenching and temperature on the sensitivity of LIF detection, although there is a reduction in the number density of the HOx species in the expansion. We report the adaptation of our time-resolved OH-FAGE instrument to allow HO_2 detection, the characterization of the instrument (including development of a calibration method for HO_2 yields of OH initiated reactions), and the investigation of the influence of RO_2 species. Finally, we discuss the application of the technique to determine the yield of HO_2 from the reaction of OH with n-butanol. The instrument has some similarities to that presented by Nehr et al. (2011) where a conventional OH lifetime instrument was altered to allow for chemical conversion of HO_2 to OH and hence the sequential determination of OH and HO_2.

2 Experimental

Reactions were carried out in a high pressure (0.5 – 5 bar) reaction cell which is described in greater detail in Stone et al. (2016) and schematics of which are shown in Figures 1 and 2. The high-pressure reactor was a 0.5 m stainless steel tube with a 22 mm internal diameter. Gas flows were delivered to the high-pressure cell from a mixing manifold where calibrated mass flow controllers (MFC) allowed for accurate control of flow rates. Low vapour pressure compounds: OH precursors (H_2O_2), and substrates methanol and butanol, were delivered to the mixing manifold

from, thermostatted bubblers in pressure regulated backing flows of nitrogen (N_2). Ethane and oxygen were delivered directly from cylinders into the mixing manifold through MFCs. The gas flowrate through the cell was kept under laminar conditions with typical Reynolds values (Re) of 480 (corresponding to a flow rate for an experiment of 10 SLM at 2 bar); in general conditions were maintained between 400-800 Re (Re < 2400 = laminar flow), with some experiments carried out with higher flowrates, up to 1800 Re.

Temperature control of the reactor between room temperature and 800 K was achieved by altering the voltage applied to a coil heater (WATROD tubular heater, Watlow) over the last 30 cm of the stainless-steel tube. The heated region was fitted with a quartz liner (inner diameter 18 mm) to reduce wall-initiated chemistry. A temperature readout, from a type K thermocouple in the gas flow, close to the pinhole, was calibrated for given flow rates, pressures and voltage settings by measuring the highly temperature sensitive OH and methane rate coefficient, using the temperature dependence reported by (Dunlop and Tully, 1993). A more detailed description of this method is described within instrument characterization (Section 3.4).

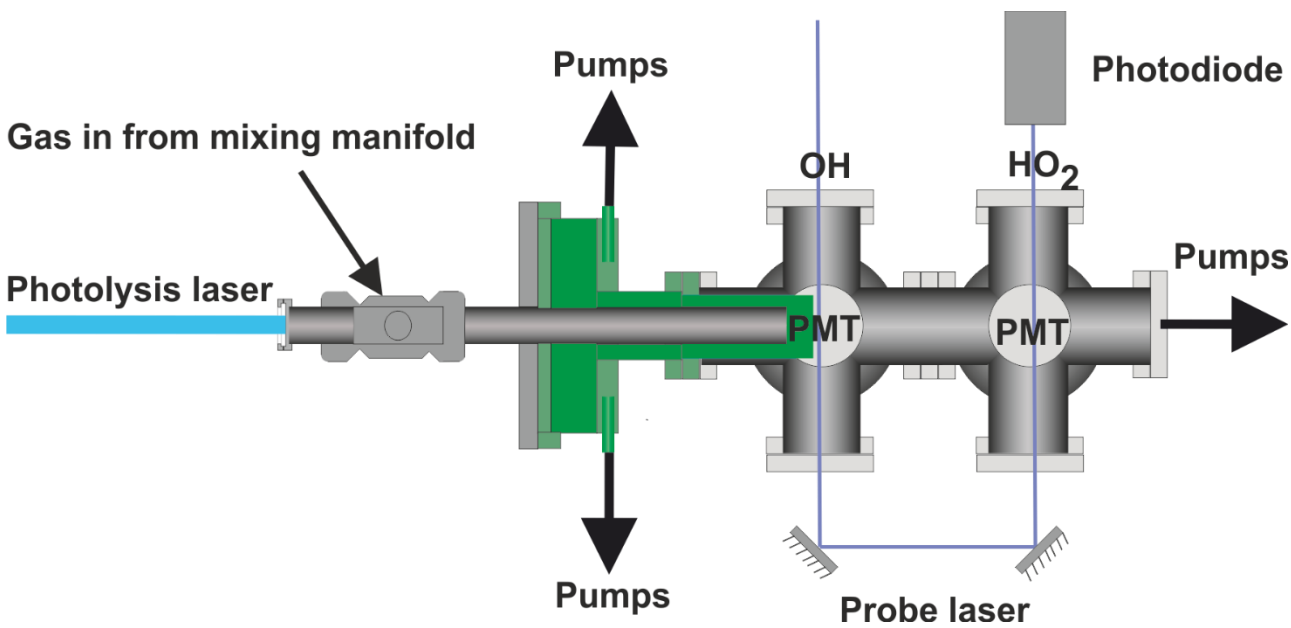

Figure 1. Schematic plan of the apparatus.

The photolysis of the OH precursor, H_2O_2, at 248 nm (Lambda Physik, Compex 200 operated using KrF at 1 or 5 Hz) or 266 nm (frequency quadrupled Nd-YAG output, Quantel, Q-

smart 850 at 1 or 10 Hz) initiated the chemistry. No significant difference was noted in the kinetics or yields as a function of laser repetition rate.

$$H_2O_2 + h\nu \rightarrow 2OH \qquad \text{(R4)}$$

Hydrogen peroxide was used as the OH precursor for all experiments where HO_2 detection was performed, because it also acts as an internal calibrant to relate OH and HO_2, via reaction R5:

$$\mathbf{OH} + H_2O_2 \rightarrow H_2O + \mathbf{HO_2} \qquad \text{(R5)}$$

However, in general, other OH precursors can be used. The OH precursor was maintained at low concentrations ($1 \times 10^{14} – 1 \times 10^{15}$ molecule cm^{-3}) to minimise errors associated with assigning pseudo-first-order kinetics for the loss of OH, and to reduce radical-radical reactions. Maintaining a low radical precursor concentration had the additional advantage of minimising attenuation of the photolysis beam, ensuring consistency in the initial radical concentrations generated along the length of the high-pressure cell. Initial OH concentrations were in the range $2 \times 10^{11} – 5 \times 10^{13}$ molecule cm^{-3}.

A pinhole (diameter < 0.15 mm) at the end of the high-pressure reactor couples the reactor to the low-pressure (0.3 – 5 Torr) detection cell. Details on OH detection can be found in Stone et al. (2016). The accuracy of the instrument for OH measurement has recently been verified by measurements of the rate coefficient of the reaction of OH with isoprene (Medeiros et al., 2018) which are in excellent agreement with the literature. A more detailed schematic for the low-pressure detection cell is shown in Figure 2.

In the first low pressure detection cell, the OH was probed within the jet expanded gas, close to pinhole (<5 mm), perpendicular to the gas flow. The OH was detected by off-resonance laser induced fluorescence (LIF) at 308 nm following excitation with 282 nm light ($A^2\Sigma$ ($v' = 1$) ← $X^2\Pi(v'' = 0)$,Q_{11}). The 282 nm light was the frequency doubled output of a dye laser ((Rhodamine 6 G, Spectron) pumped at 532 nm by a Nd:YAG laser (Spectron), or (Rhodamine 6 G, Continuum) pumped by a Nd-YAG laser (Quantel, Q-smart 850)). Measuring the off-resonance fluorescence allowed the use of a filter (308 ± 5 nm, Barr Associates) before the photomultiplier (Perkin-Elmer C1943P) to remove scattered light and improved the signal to noise ratio.

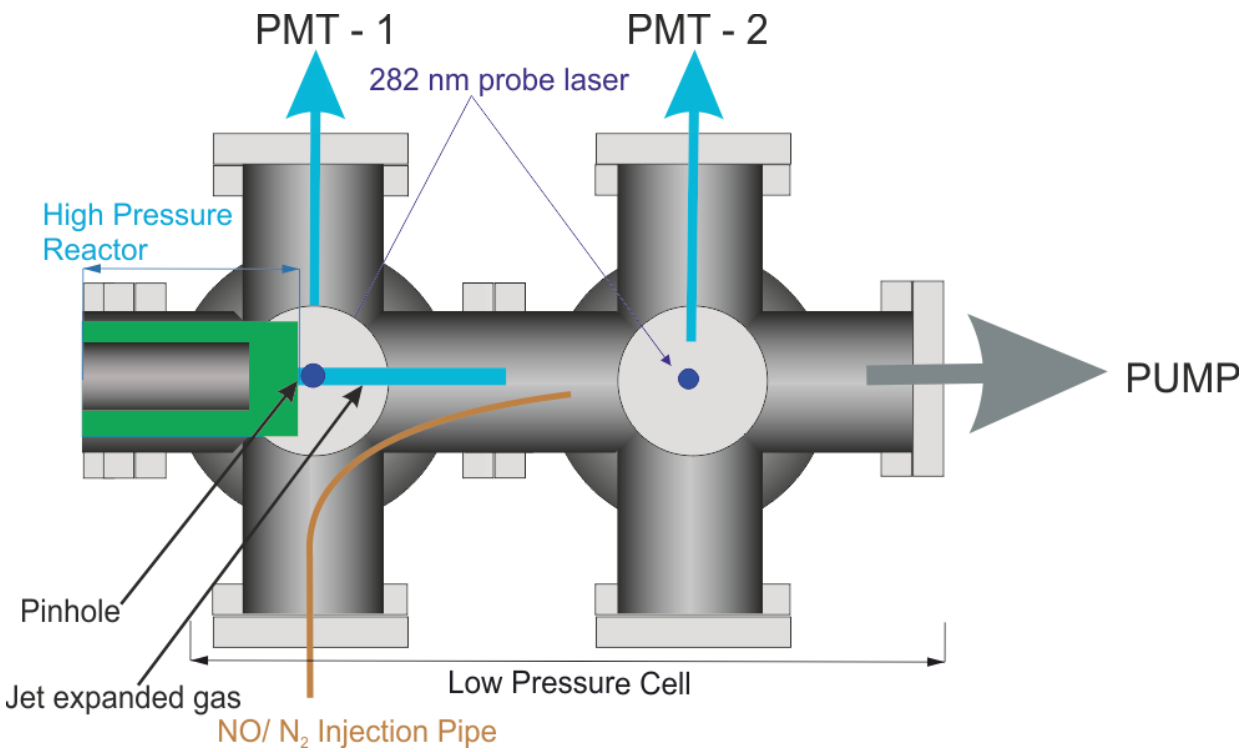

Figure 2. Detailed schematic elevation of the low-pressure detection region of the reactor. The blue line represents the jet expanded gas; the jet breaks down after approximately 2 cm. NO was injected through a 1.5 mm id stainless steel tube after the breakdown of the jet.

A delay generator (BNC DG535) was used to vary the delay (time resolution ~10 ns) between the photolysis and probe laser, facilitating generation of time profiles of the OH concentration. The traces, typically 200 – 300 data points and ranging in time from ~50 µs – 20 ms, were scanned through multiple times (5 – 20) and the signal at each time point was averaged, giving high precision OH loss traces. An example OH trace from the first detection cell for reaction R5 is presented in Figure 3. As reactions were carried out under pseudo first order conditions ([OH] << [substrate]), the time dependence of the OH LIF signal, I_f, (proportional to the [OH]) was given by:

$$I_{f,t} = I_{f,0} e^{-k_{\mathrm{OH}} t}$$

where $k_{\mathrm{OH}} = k_5[H_2O_2]$. In Figure 3 two traces are presented from the first, OH, detection axis, these two traces were taken in consecutive experiments with a constant $[H_2O_2]$ where the first trace ($k_{\mathrm{OH,1st}}$ = (2351 ± 22) s^{-1}) was taken where N_2 was flowed into the low pressure region, the second

trace ($k_{OH,1st}$ = (2389 ± 18) s^{-1}) was taken when this flow had been switched to NO to allow HO_2 detection in the second detection cell, errors are given as 2 σ. The similarity of the OH decay traces when either N_2 or NO was injected shows that there was no back streaming of NO in the low-pressure cell and hence no HO_2 conversion at the first detection axis.

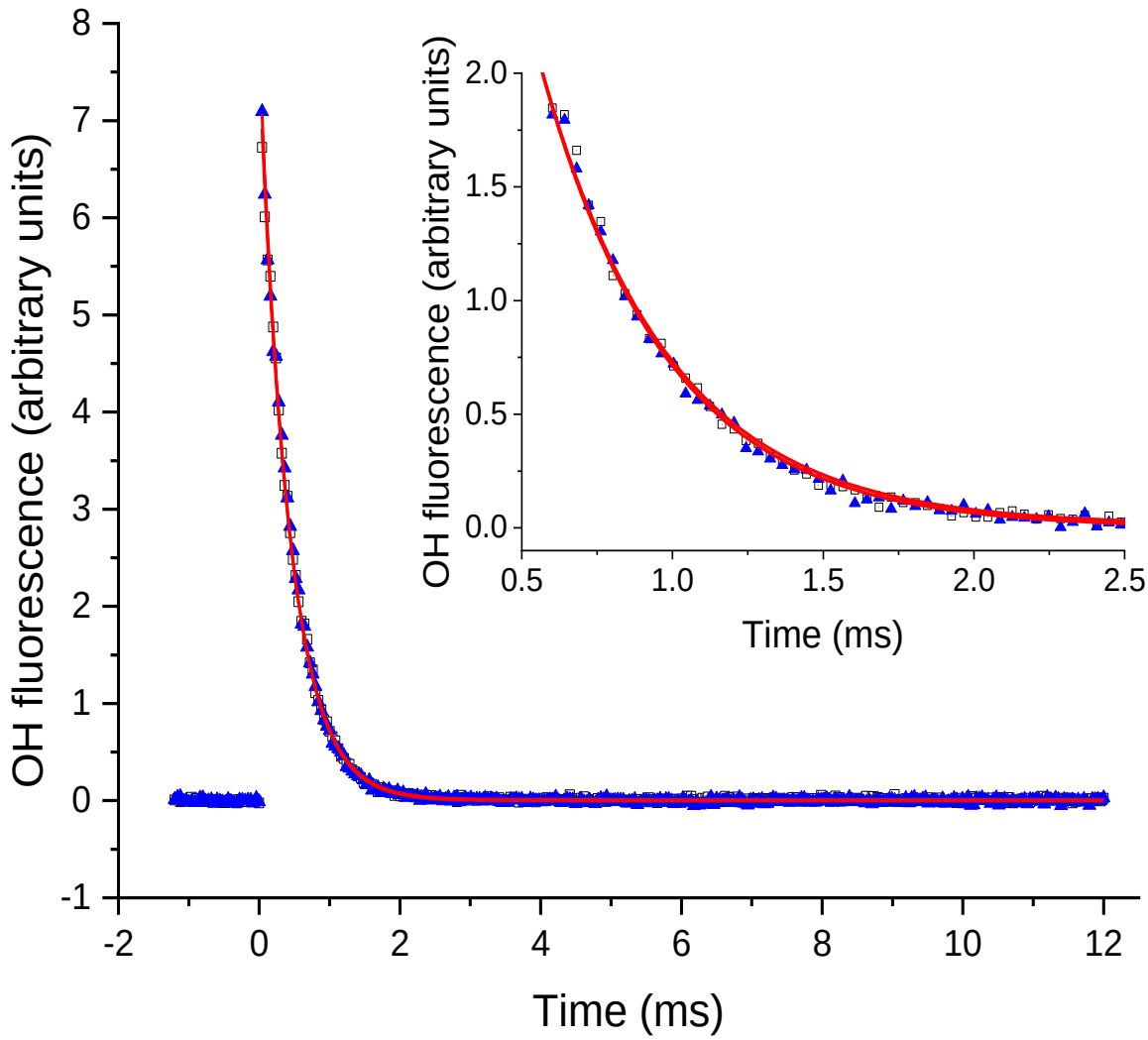

Figure 3. An example of the OH signal (solid blue triangles) collected at the first detection axis for the reaction of OH with H_2O_2 ([H_2O_2] ≈ 1.4 × 10^{15} molecule cm^{-3}, with a flow of N_2 into the low-pressure cell, with open black squares representing the subsequent trace taken with a flow of NO. The red lines represent the non-linear least squares fits to an exponential decay ($k_{OH,1st}$ = (2351± 22) s^{-1} and $k_{OH,1st}$ = (2389 ± 18) s^{-1}), 2 σ errors.

HO_2 radicals were monitored by the chemical transformation of HO_2 to OH via reaction with NO (R3) in the low-pressure cell. Following the breakdown of the jet, after the Mach disk (>2 cm beyond the pinhole), a small flow (5 sccm) of NO or N_2 was introduced into the low-pressure cell via a 1.5 mm i.d. stainless steel pipe (for a typical 0.5 Torr pressure in the FAGE cell the NO concentration was 5.5×10^{13} molecule cm^{-3}). After passing through the first detection cell, the probe beam was redirected through the second low-pressure detection cell downstream of the NO pipe allowing for the measurement of the OH concentration by LIF in the same manner as in the first cell.

By switching between a flow of N_2 and NO, through the pipe, traces for OH loss and HO_2 formation could be elucidated, examples of which are shown in Figure 4. Subtraction of the two OH traces in Figure 4, (upper, red trace is with NO injection and the signal corresponds to reactant OH and OH produced from the titration of HO_2 to OH, lower, blue trace with N_2 injection is reactant OH only) gave a resultant signal associated with HO_2 production in the high-pressure reactor, shown the pink trace in Figure 4. The signal from the first PMT allowed for correction of the signal heights at the second PMT for changes in the probe laser power or wavelength, any variations in laser power or wavelength affect the absolute signal retrieved from both PMTs; however, the relative signals retrieved from the PMTs remain consistent.

Fits to the HO_2 formation traces and OH loss traces from the second cell generated kinetic parameters which differed from the accurate parameters collected at the first detection axis, $k_{OH,2nd} = (1390 \pm 44)\ s^{-1}$ and $k_{HO2,2nd} = (1080 \pm 150)\ s^{-1}$ where the accurate loss parameters from the first cell were $k_{OH,1st} = (2389 \pm 18)\ s^{-1}$, 2 σ errors. This difference was the result of transport effects. By comparison of the loss and formation parameters derived for OH + H_2O_2, for the first and second detection cells, HO_2 formation rates could be assigned from a calibration plot (Figure 7).

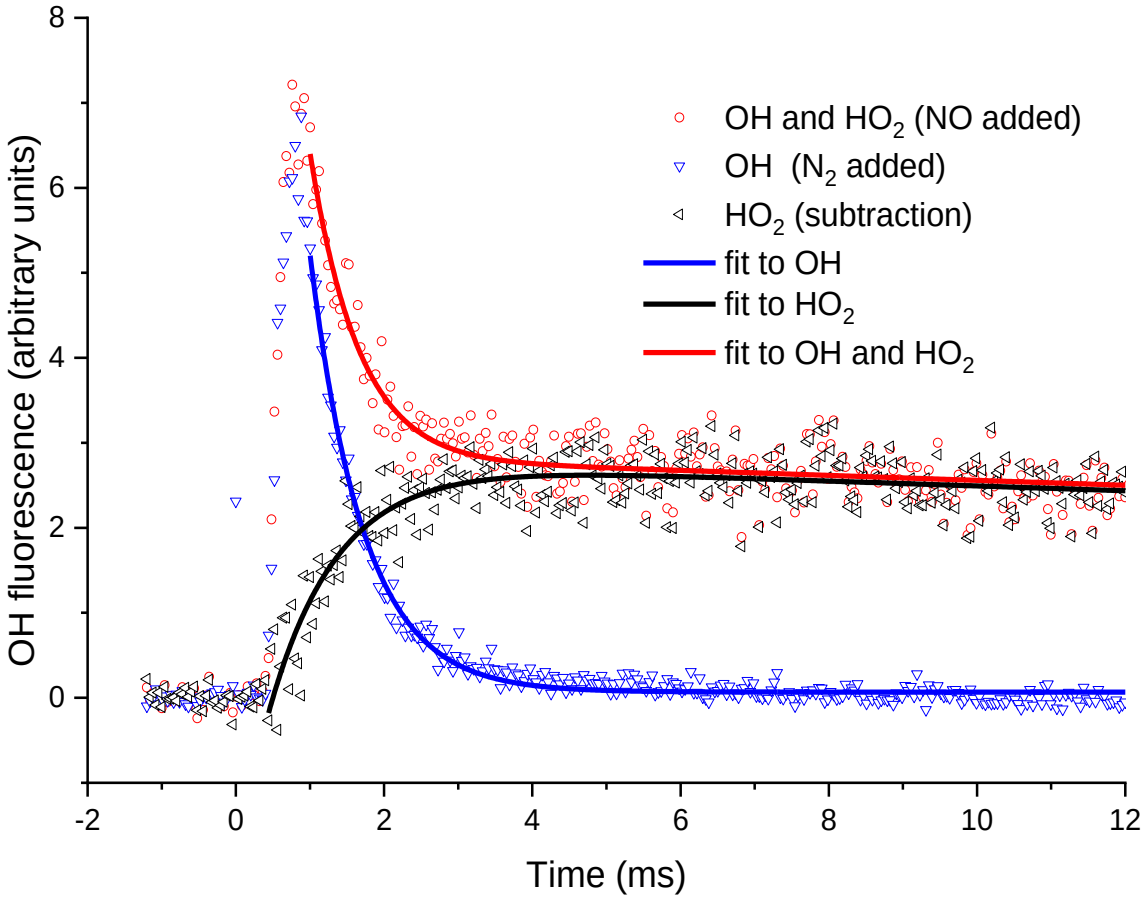

Figure 4. Examples of OH fluorescence traces collected at the second detection axis under the same conditions for Figure 3. The blue triangles are where N_2 has been injected through the pipe, i.e. no HO_2 to OH conversion. The OH signal profile differs from that in Figure 3, with $k_{OH,2nd}$ = (1390 ± 44) s^{-1} (2 σ errors), additionally, there is a time-delay to peak OH, representing the transport time (primarily the time taken to travel from the breakdown of the jet to the second detection axis). The red circles are the OH signal obtained with NO injection. At short times the signal is dominated by reactant OH, but at times greater than 2 ms, the signal is dominated by OH titrated from the HO_2 product. The resultant OH trace associated with HO_2 formation in the high-pressure cell obtained by subtracting the two OH traces, obtained with either NO or N_2 injection prior to the second detection axis, shown as black triangles, a biexponential growth and decay fit, black curve, gave a formation rate coefficient, $k_{HO2,2nd}$ = (1080 ± 150) s^{-1} (2 σ error).

Neither of the OH determinations in the two detection axes provide absolute measurements of radical concentrations. Each detection axis could be calibrated as for chamber measurements, but for our purposes a calibration reaction linking photolytically produced OH and HO_2 removes

many sources of error compared to an absolute calibration. The reaction of OH with the radical precursor H_2O_2 which directly forms HO_2 with a 100 percent yield was used for calibration.

$$\mathbf{OH} + H_2O_2 \rightarrow H_2O + \mathbf{HO_2} \qquad \textbf{(}\text{R5})$$

For reactions carried out where a reagent was added in addition to the H_2O_2, the resulting ratios can be compared with those from the calibration reaction to allow assignment of an observed HO_2 yield. To assign the HO_2 yield from the test reaction required accounting for secondary HO_2 production in the high-pressure reactor, from OH + H_2O_2 and photolysis processes. From the known rate coefficients, it was possible to calculate the fraction of OH reacting with the H_2O_2 (typically 5 – 10%) and hence the expected contribution to the HO_2 signal. Photolytic production of HO_2 was accounted for by measuring the observed HO_2 signal in the absence of any H_2O_2.

In a typical experiment, the reaction of OH and H_2O_2 would be carried out four times, twice in the absence of NO and twice with the addition of NO to calibrate the instrument. Exponential fits to the OH decay as monitored in the first cell determine the peak OH signal. The OH signals at the second detector recorded with only N_2 addition (reagent OH reaching the second detector) and subtracted from the signal with NO added (reagent OH and HO_2) to give the net HO_2 signal. This profile was fitted to, a biexponential growth and decay function, to extract the peak HO_2 signal for that set of conditions. Combinations of traces were then used to obtain an averaged value (and uncertainty) of the signal on the first PMT (OH) to the net HO_2 signal at the second PMT for this calibration reaction where OH reactant and HO_2 product have a 1:1 relationship. The same process was then performed in the presence of the compound of study. The removal pseudo-first-order rate coefficient with H_2O_2 and the reagent of study ($k'_{OH,1st} = k_{OH+H2O2}[H_2O_2] + k_{OH+TEST}[TEST]$) was compared to the removal pseudo-first-order rate coefficient with only H_2O_2 ($k'_{OH,1st} = k_{OH+H2O2}[H_2O_2]$) to assign what fraction of the OH reacted with the H_2O_2 precursor and hence the resulting contribution to the observed HO_2. Comparison of the remaining peak ratio to the ratio from the H_2O_2 and OH calibration experiment provided the experimentally derived HO_2 yield for reaction of OH and the reagent of study.

Branching ratios to direct HO_2 formation could be assigned with an accuracy of ~10 %, the limitations to this were signal to noise effects, where improved signal to noise could be achieved by increasing the precursor concentration and photolysis energy. However, this was limited by the

need to ensure pseudo-first-order conditions were maintained and to minimize radical-radical processes. Ensuring the dominant reaction was between OH and the reagent of study, whilst still being able to accurately measure the initial OH conditions, provided a limit to the maximum removal rates achievable ($k_{OH,1st}$ < 30,000 s^{-1}).

3 Instrument Characterization

Many reactions of atmospheric and combustion interest are studied in the presence of oxygen leading to the generation of peroxy radicals (RO_2). For certain RO_2 there is a potential to generate OH and HO_2 on a fast timescale and therefore three well known reactions were chosen to characterize the instrument, OH and ethane, OH and ethylene, and OH and methanol.

$$OH + C_2H_6 \rightarrow H_2O + C_2H_5 \quad \text{(R6)}$$

$$OH + C_2H_4 \rightarrow HOC_2H_4 \quad \text{(R7)}$$

$$OH + CH_3OH \rightarrow H_2O + CH_2OH,\ CH_2OH + O_2 \rightarrow HO_2 + HCHO \text{ (fast)} \quad \text{(R8a, R9)}$$

$$OH + CH_3OH \rightarrow H_2O + CH_3O,\ CH_3O + O_2 \rightarrow HO_2 + HCHO \text{ (slow)} \quad \text{(R8b, R10)}$$

OH and ethane (R6) gives an assessment of any false yields generated from RO_2 and NO from prototypical alkyl RO_2 species that will be formed from many atmospherically relevant reactions. Ethylene and OH (R7) forms a hydroxy alkyl peroxy radical, the typical RO_2 species known to create interferences in FAGE HO_2 detection systems (Fuchs et al., 2011;Hard et al., 1984;Whalley et al., 2013). Minimizing and understanding the HO_2 yield from this reaction allowed for limits to the selectivity of the instrument to be known. The reaction of OH with methanol is a well understood reaction; the two isomeric radical products react with oxygen on differing timescales to generate HO_2. Complete conversion of both isomers should yield 100 % HO_2.

As discussed in the experimental section, transport effects after the breakup of the sampling jet mean that rate coefficients measured in the second cell $k_{X,2nd}$ (X = OH or HO_2) differ from each other (transport effects scale with mass) and from those made in the first detection axis ($k_{OH,1st}$). Pseudo-first-order rate coefficients from the two detection axes were compared to ascertain whether measurements in the second detection axes can be used to make quantitative kinetic measurements.

Finally, the layout of the apparatus makes it hard to accurately measure the temperature at which the reaction occurs; for reactions occurring on a millisecond timescale, the relevant reaction distance from the sampling pinhole is approximately 0.05 - 0.5 mm. Compared to a conventional slow flow laser flash photolysis/laser induced fluorescence apparatus, where the reaction volume is the overlap of the perpendicular photolysis and probe laser beams, it is hard to accurately position the thermocouple and additionally, any thermocouple located close to the sampling pinhole may affect the flow into the low pressure system. In addition to the difficulties in correctly siting a thermocouple, there are additional errors (flow, conduction and radiative) that derive from measuring the temperature of a flowing gas with a thermocouple. We have therefore performed additional experiments to determine the temperature based on the well characterized and temperature sensitive reaction of OH and methane.

3.1 Interference by RO_2 species

Selectivity in measuring HO_2 concentrations plays an important role in the viability of detection methods for monitoring reactions important for atmospheric chemistry. At high pressures, the reaction of NO with many atmospherically relevant RO_2 species in the presence of oxygen induces HO_2 formation. By performing the titration in the low-pressure cell with the NO + HO_2 reaction under 'starved NO' conditions minimized this effect. This premise was validated by measuring the OH + ethane and OH + ethylene HO_2 yields under high oxygen conditions. In our system the typical oxygen concentrations in the high pressure reactor were varied between 1×10^{16} and 5×10^{17} molecule cm^{-3} which led to concentrations in the low pressure cell of 3×10^{12} to 2×10^{15} molecule cm^{-3}.

The reaction of OH + ethane (R6) under high oxygen conditions permits the rapid formation of the ethylperoxy radical, which is an RO_2 radical that has a typical slow, NO propagated, route to HO_2 formation (R11 – R12).

$$CH_3CH_2O_2 + NO \rightarrow CH_3CH_2O + NO_2 \quad \text{(R11)}$$

($k_{11,\,298\,K} = 8.70 \times 10^{-12}$ cm^3 $molecule^{-1}$ s^{-1}) (Atkinson et al., 2006)

$$CH_3CH_2O + O_2 \rightarrow CH_3CHO + HO_2 \quad \text{(R12)}$$

($k_{12,\,298\,K} = 9.48 \times 10^{-15}$ cm^3 $molecule^{-1}$ s^{-1}) (Atkinson et al., 2006)

Under a variety of NO flows the apparent HO_2 yield for the OH + C_2H_6 system was 3 ± 6 %, which indicates that for most reactions carried out in our system, chemical transformation by reaction with NO, was sensitive to HO_2 rather than RO_2 species, where the RO_2 radical was the product of O_2 addition to a simple alkyl radical.

The reaction of ethylene and OH (R7) in the presence of oxygen forms the hydroxyethylperoxy radical ($HOCH_2CH_2O_2$), and reaction of the $HOCH_2CH_2O_2$ with NO in the presence of O_2 provides a route for the prompt regeneration of OH. For this reaction, an apparent HO_2 yield of 100 ± 15 % was observed; however, by varying the concentration of NO added to low pressure cell (between 5×10^{13} and 5×10^{14} molecule cm^{-3}), the formation rate of OH was reduced minimizing the apparent yield observed (<70 %) and slowing the observed rate of OH regeneration (<1000 s^{-1}).

$$HOCH_2CH_2O_2 + NO \rightarrow HOCH_2CH_2O + NO_2 \quad \text{(R13)}$$

($k_{13,\,298\,K} = 9.00 \times 10^{-12}$ cm^3 $molecule^{-1}$ s^{-1}) (Atkinson et al., 2006)

$$HOCH_2CH_2O \rightarrow CH_2O + HOCH_2 \quad \text{(R14)}$$

($k_{14,\,298\,K} = 1.3 \times 10^{5}$ s^{-1}) (Orlando et al., 1998)

$$CH_2OH + O_2 \rightarrow CH_2O + HO_2 \quad \text{(R9)}$$

($k_{9,\,298\,K} = 9.60 \times 10^{-12}$ cm^3 $molecule^{-1}$ s^{-1}) (Atkinson et al., 2006)

For test reagents which can generate radicals similar to hydroxyethylperoxy, our instrument will detect both HO_2 and RO_2 with some selectivity to HO_2. Potential RO_2 interference can be tested by examining the 'HO_2' yield as a function of added [NO].

3.2 OH + methanol

To verify the accuracy of the method for determining HO_2 yields the reaction of OH and methanol (R8) was examined. The branching ratio for the α abstraction to yield CH_2OH (R8a) reported by the IUPAC evaluation and based on the experimental data of McCaulley et al. (1989), is α = (85 ± 8)% at room temperature with the methoxy yield as (15 ± 8)%. Reaction R8 was studied at room temperature with the reaction being initiated by the photolysis of H_2O_2 at 248 nm. In the presence of low concentrations of oxygen (< 1×10^{16} molecule cm^{-3}), the α abstraction still leads to prompt formation of HO_2 via R9, but R10, $CH_3O + O_2$, occurs on a much longer timescale

(the ratio $k_{9,298\ K}$:$k_{10,\ 298\ K}$ is ~5000 (Atkinson et al. 2006)) and is not observed under these conditions. The observed HO_2 yield, (87 ± 10)% (first row of Table 1) gives the fraction of reaction R8 forming CH_2OH and the value is consistent with the IUPAC evaluation.

Table 1. HO_2 yields from the reaction of OH with CH_3OH with varying [O_2] carried out 295 K. Errors given as 2 σ.

[O_2]/ molecule cm^{-3}	HO_2 Yield (%)				Average HO_2 Yield (%)
	Expt 1	Expt 2	Expt 3	Expt 4	
$<1 \times 10^{16}$	90	89	79	88	(87 ± 10)
$>2 \times 10^{18}$	93	94	100	99	(97 ± 6)
6×10^{18}	103	97	101	97	(99 ± 2)
6×10^{18}	98	102	98	98	

When higher concentrations of oxygen are used, the timescale for HO_2 production from reaction R10 decreases and now both abstraction channels lead to HO_2 detection in our apparatus. The resulting observed yield (final three rows of Table 1) is consistent with 100% conversion of OH to HO_2 and is statistically different from the low oxygen measurements based on a Welch t-test at the 98% level. The reproduction of the literature HO_2 yields from the reaction of OH with methanol under varying [O_2] demonstrates that the instrument can accurately measure HO_2 yields with good precision. It has additionally been demonstrated that the instrument had sufficient accuracy and precision to assign the branching ratios for differing abstraction channels when it was possible to separate the channels by the timescale for HO_2 generation.

A possible interference that could distort the yield of HO_2 is the role of the radical-radical reaction OH + HO_2 (Assaf and Fittschen, 2016):

$OH + HO_2 \rightarrow H_2O + O_2$ $\quad k_{15} = 1.1 \times 10^{-10}$ cm^3 $molecule^{-1}$ s^{-1} Atkinson et al. (2006) (R15)

At the low radical concentrations used in many experiments in this work, this reaction could contribute 5 – 10% of the OH loss in an OH + H_2O_2 calibration experiment. However, we have looked at the dependence of the HO_2 yield from both OH/H_2O_2 and from OH/CH_3OH, but see no

significant effects of secondary radical-radical reaction (<5%) as the calculated $[OH]_0$ is changed from 5×10^{11} to 5×10^{12} molecule cm^{-3}. For the OH/CH_3OH the much larger concentrations of substrate used lead to faster pseudo-first order decays, so radical-radical contribution is significantly reduced. The work of Assaf and Fittschen suggests that a more significant deviation in the OH loss rates, and one that we ought to be to detect given the precision of our data, should be observed. It is possible that our calculations of $[OH]_0$ are over-estimated, but we note that a study of the OH + H_2O_2 reaction by Wine et al. (1981), where they specifically looked for the interference on OH decays from R15, could find no evidence for an increase in the loss of OH, when $[HO_2]$ was artificially increased.

3.3 Assessment of transport effects on observed kinetics

Due to the differing conditions in the two detection regions, the kinetics observed at the first detection axis, where OH LIF was performed in the jet-expanded gas, and in the second detection region, where LIF is performed 15 cm downstream from the pinhole after the breakdown of the jetting gas, will be treated separately. For validating the accuracy of the OH kinetics in the first cell, the reactions of OH and methane (CH_4) (Dunlop and Tully, 1993), OH and ethylene (C_2H_4) (Atkinson et al., 1982;Tully, 1983) were studied. The high accuracy and precision of this system for measuring OH kinetics has further been demonstrated in a recent publication on the reaction of OH and isoprene (C_5H_8) (Medeiros et al., 2018).

$$OH + CH_4 \rightarrow H_2O + CH_3 \qquad (R16)$$

$$OH + C_2H_4 \rightarrow HOC_2H_4 \qquad (R7)$$

$$OH + C_5H_8 \rightarrow HOC_5H_8 \qquad (R17)$$

When these reactions were carried out at room temperature the expected bimolecular rate coefficients could be reproducibly accurately measured for observed rate coefficients less than 150,000 s^{-1}.

Studies on the reaction of OH and ethylene at room temperature and 2.2 bar, shown in Figure 5, gave a value of $k_7 = (8.33 \pm 0.16) \times 10^{-12}$ cm^3 $molecule^{-1}$ s^{-1} (2σ errors) which matched well with literature high pressure limits for OH and ethylene; where a direct pulsed laser photolysis

laser induced fluorescence study by Tully (1983) gave k_7 = (8.47 ± 0.24) × 10^{-12} cm^3 $molecule^{-1}$ s^{-1}, and a relative rate study by Atkinson et al. (1982) found k_7 = (8.11 ± 0.37) × 10^{-12} cm^3 $molecule^{-1}$ s^{-1}. However, for pseudo-first order rate coefficients above ~150000 s^{-1}, there was no longer a linear dependence of the rate coefficient with reagent concentration; transport effects are becoming significant even for OH detection in the jetting region.

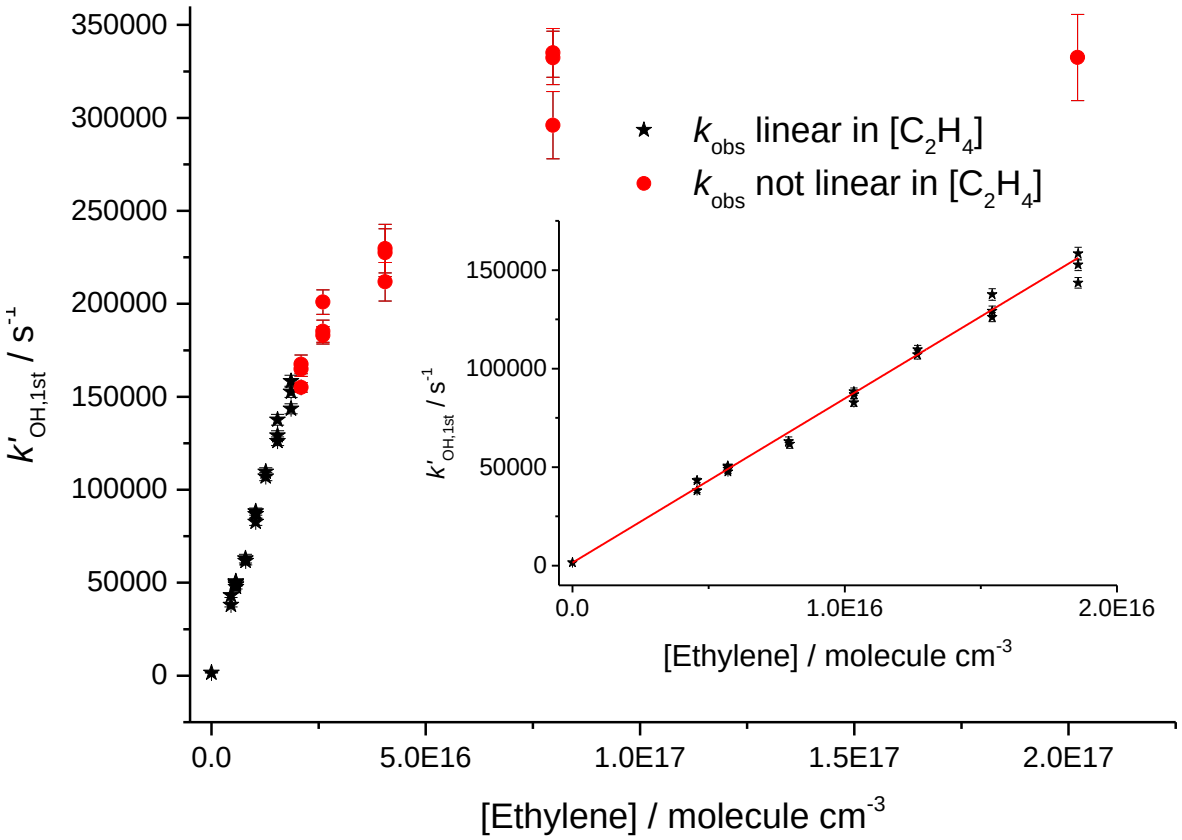

Figure 5. Bimolecular plot of the pseudo-first-order rate coefficient at the first detector, $k'_{OH,1st}$, vs ethylene concentration. The figure demonstrates a linear relationship below ~150,000 s^{-1} (see inset for detail in linear region) but with increasing curvature, due to transport effects at higher values of $k'_{OH,1st}$. Black stars symbolize where $k'_{OH,1st}$ was linear with [C_2H_4], red circles where $k'_{OH,1st}$ showed greater than 5% deviation from linearity.

The OH traces detected in the second cell deviated from those observed from the first cell, as shown in Figures 3 and 4. There is understandably an increased time delay from time zero (the photolysis laser pulse) to arrival of OH radicals at the second detection axis due to the increased distance travelled after sampling (> 150 mm versus < 5 mm). Additionally, the arrival of OH to

the second axis is spread out further in time due to transport issues relating to non-linear flow conditions at the breakdown of the jet, and the arrival of the OH being affected by its velocity distribution (Moore and Carr, 1977;Taatjes, 2007;Baeza-Romero et al., 2012). Figure 6 shows a plot of observed OH rate coefficient from the first detection axis ($k_{OH,1st}$) against observed rate coefficient from the second axis ($k_{OH,2nd}$) in the reaction of OH with H_2O_2. For values of k_{OH} below 2500 s^{-1} it was possible to accurately assign an expected OH removal rate for reactions observed in the second cell ($k_{OH,2nd}$) given the observed OH kinetics at the first detection axis ($k_{OH,1st}$). This is useful to compare the kinetics of OH removal and HO_2 production.

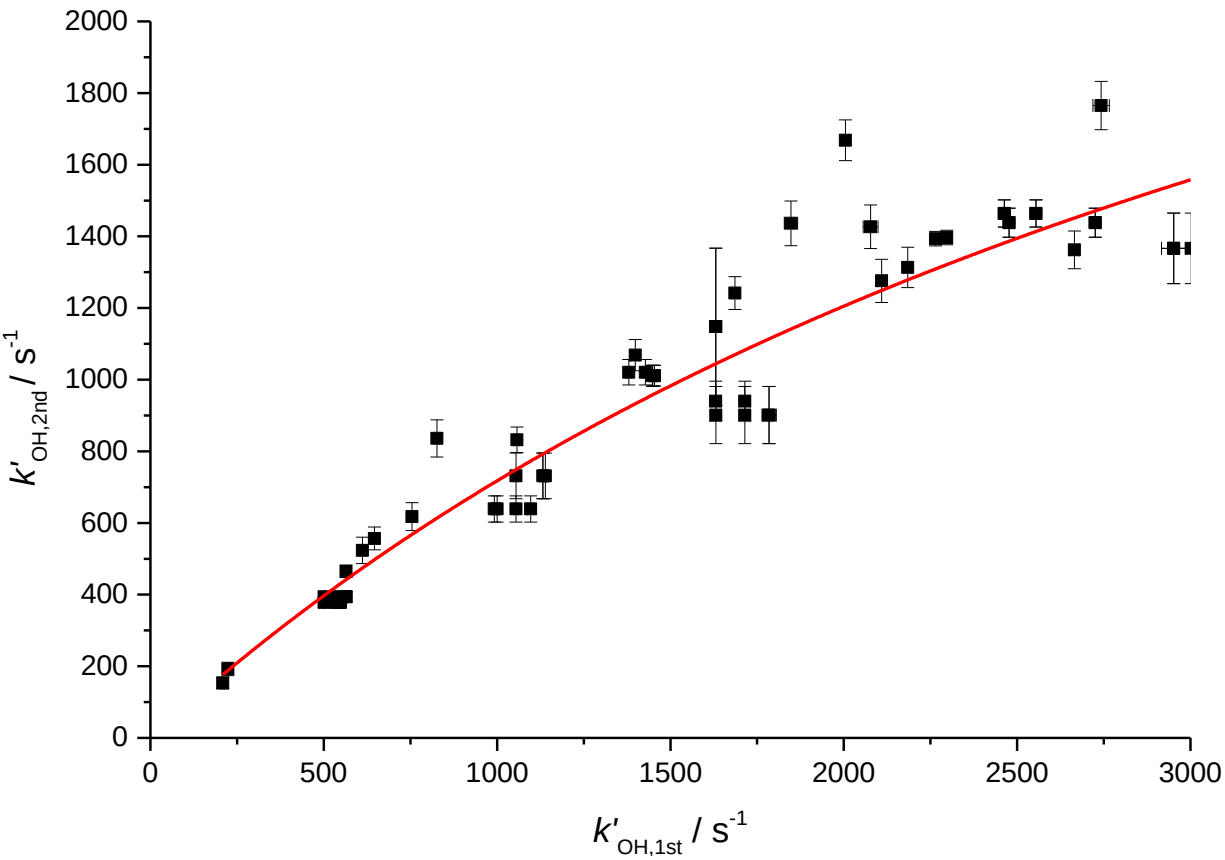

Figure 6. Relationship between the observed rate coefficient for the reaction of OH with H_2O_2 observed in the first cell ($k_{OH,1st}$) and the observed OH removal rate in the second cell ($k_{OH,2nd}$). The difference is non-linear but a simple fit to this could be used to assign removal rates to traces observed in the second cell below 2,500 s^{-1}. The red line is the simplified fit of the form, $y = A * (1 - e^{-b*x})$, where A was some limit value above which no increase in measured rate coefficient would be observed.

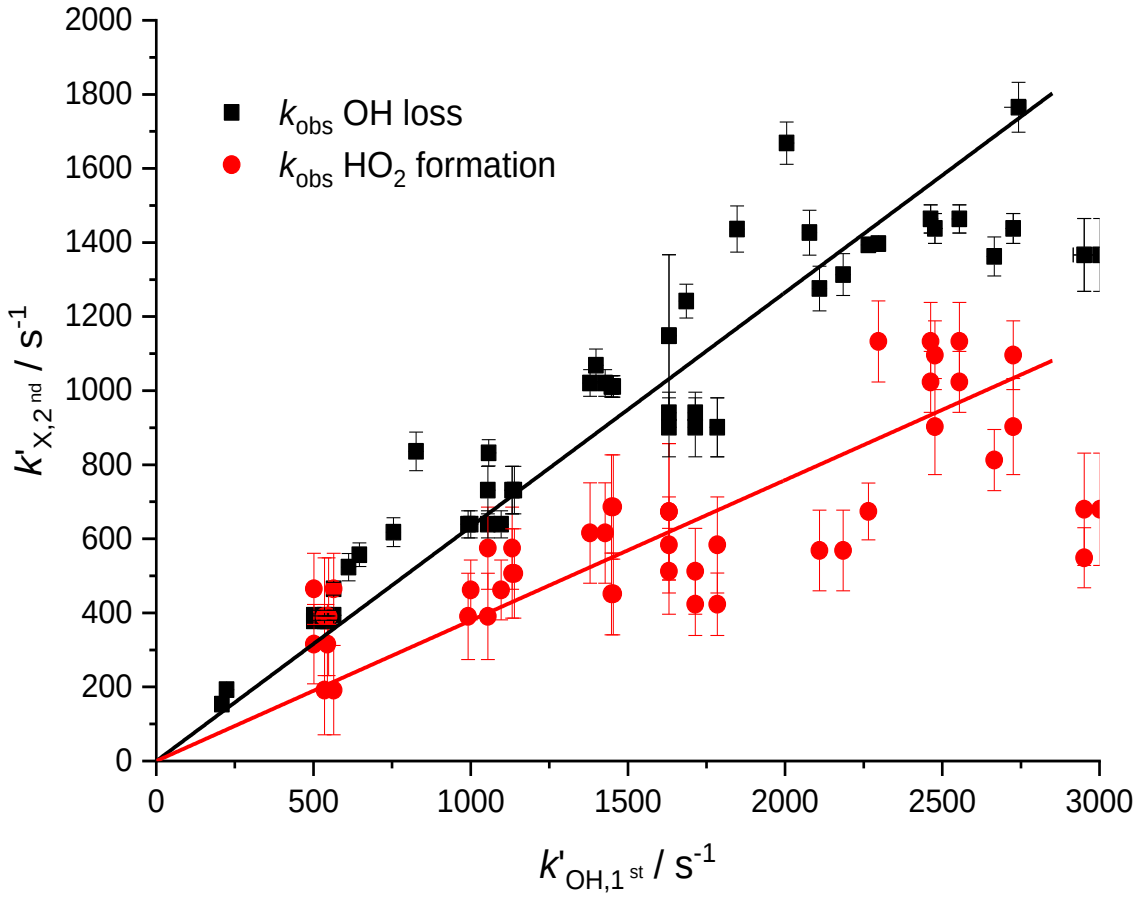

Figure 7. Relationship between the pseudo-first-order rate coefficient for OH loss observed in the first cell ($k'_{OH,1st}$) from the reaction of OH with H_2O_2 and the observed rate coefficients measured in the second cell ($k'_{X,2nd}$ where X = OH loss (black squares, ■) or HO_2 production (red circles, ●)) a non-linear fit can be used to assign removal rates and HO_2 formation rates to traces observed in the second cell below 2,500 s^{-1}.

As the observed kinetics in the second cell are significantly affected by the velocity distribution of the species being detected, there is again a deviation between the observed kinetics expected from the measurement of the OH radicals loss and the kinetics for HO_2 formation due to the differing masses of OH and HO_2. Figure 7 shows the pseudo-first order rate coefficients for OH removal ($k'_{OH,2nd}$) and HO_2 production ($k'_{HO2,2nd}$) from the OH + H_2O_2 reaction determined at the second detection axis, plotted against the OH removal at the first detection axis. The two fits to the data shown in Figure 7 had a ratio of gradients concordant with the root of the masses for HO_2 and OH, 0.60 ± 0.14 versus the expected relationship of 0.73. As with Figure 6, it is possible

to establish a calibration graph that relates the kinetics of HO_2 production at the second detection axis with the primary kinetics taking place in the high pressure reactor. This means that the timescale over which the HO_2 yield was observed could be assigned and therefore it is possible to attribute HO_2 yields to fast processes, intramolecular RO_2 decompositions or R + O_2 reactions, or to slower radical-radical reactions.

3.4 Temperature corrections

It is difficult to know the exact temperature at the pinhole as introducing a thermocouple close to the region will affect the flows and cannot be used in routine operation. A translatable thermocouple was passed along the axis of the high-pressure reactor over a variety of temperatures and showed that the temperature of the gas at the pinhole varies with axial location. In addition, radial profiles showed that in our system there was insufficient heating length to achieve uniform radial heating of the laminar gas. From the axial measurements it was observed that slower flow rates (< 5 SLM) allowed for reduced axial temperature gradients. However, these measurements showed that the only manner to achieve an even thermal profile would be a static cell.

A permanently seated thermocouple was placed perpendicularly to the flow, close to the sampling region, measurements from this thermocouple were then compared with temperature assignments from the reaction of OH and methane using the temperature dependence assigned by Dunlop and Tully (1993). This was performed over a range of heater settings and flows to allow for temperature assignment. This method was also applied to a standard low-pressure cell where the flows can be reduced to slow enough flows that thermocouple measurements could accurately define the temperature to verify the method. Additionally, the well-determined OH + ethylene adduct formation equilibrium was measured over a range of temperatures to provide an additional verification of the temperature assignment.

The method to assign a temperature from the reaction of OH and methane used the pseudo-first order rate coefficients ($k'_{OH,1st}$) measured at the first detection axis over a range of added methane flows. An estimate of the temperature was made from the thermocouple measurement, this estimated temperature was used, along with the pressure in the reactor, to calculate the added methane concentration. Comparing the predicted pseudo-first-order rate coefficient that this

estimated concertation provided using the literature value of k_{OH+CH4} (Dunlop and Tully, 1993) to the measured rate coefficient produced a difference for each point. The estimated temperature was then iteratively changed to minimize the difference between estimated and measured rate coefficients. For this minimum value, the difference between thermocouple measurement and actual temperature was tabulated against the voltage setting for the heater. A parameterization of voltage versus temperature difference was used to estimate the temperature of the reactor for experiments where no OH and methane measurements were performed and has been shown to reliably predict the temperature of the reactor within 7 K when measurements have been made subsequently.

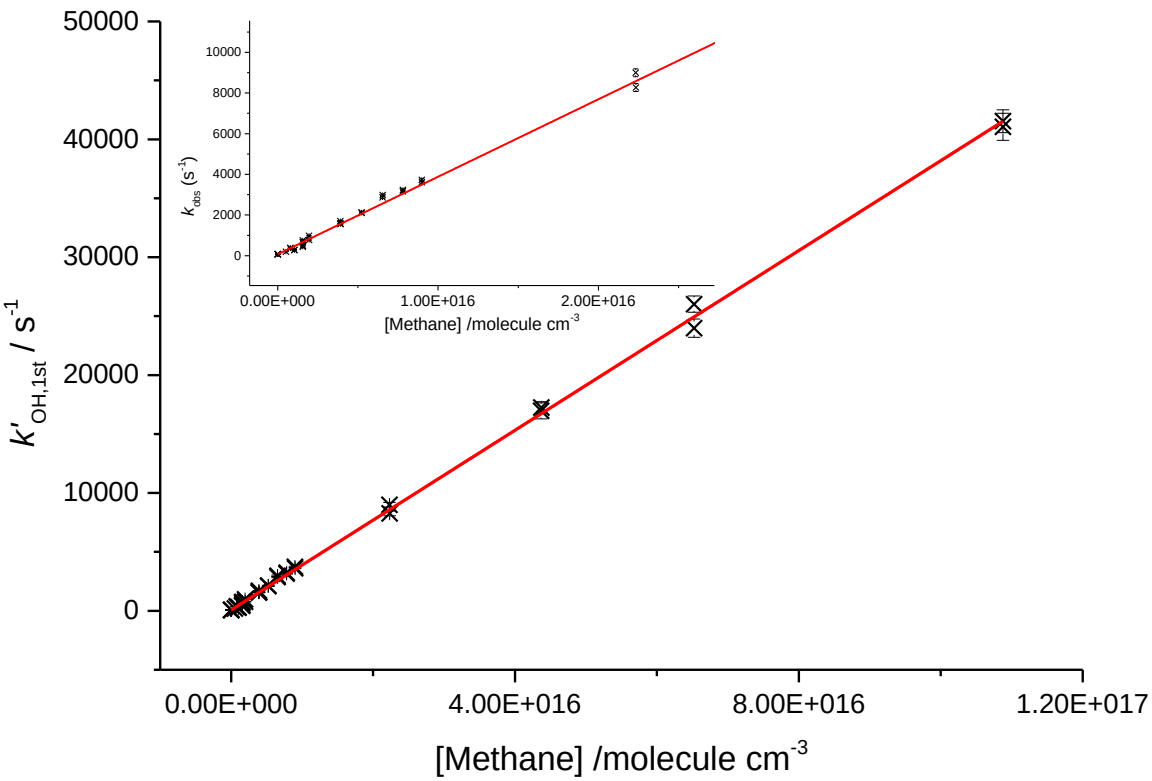

Figure 8. Bimolecular plot for the reaction of OH and methane at 680 K, 1760 Torr using 193 nm photolysis of water as an OH precursor. Here the inset shows that even at removal rates < 1000 s^{-1} the plot is still linear, indicating that within the measured experimental timescales there is little deviation in temperature.

To assess the axial temperature gradients in the gas sampled through the pinhole over the timescales of reactions measured, OH and methane rate coefficients were measured using photolysis of water at 193 nm as a source of OH. Using water photolysis allowed for low removal rates of OH by precursor and assignment of OH and methane over a range of pseudo-first-order rate coefficients ($k'_{OH,1st}$) 100 – 40000 s^{-1} as shown in Figure 8. This was performed at two temperatures (505, 680 K), and the slope of observed OH removal rate coefficients against concentration of methane appeared linear over the full range for both temperatures, thus verifying that over the distances sampled within experimental timeframes there is a minimal temperature gradient.

4 Determination of Site Specific Rate Coefficients for the Reaction of OH with n-butanol

The branching ratios for the sites of OH attack on n-butanol, as presented in Scheme 2, are of significance to the modelling of the ignition delay times for n-butanol (Agbro et al., 2017). Abstractions at the α and OH positions are chain terminating reactions at low temperatures due to the formation of the relatively inert HO_2 radical, and abstraction at the β site leads to chain propagation, through OH recycling. The new instrument permitted determination of the attack at the α and β sites; attack at the α site leads to prompt HO_2 formation in the presence of O_2; at elevated temperatures biexponential fits to non-single exponential OH loss traces in the absence of O_2 (due to decomposition of the β hydroxy radical to OH and iso-butene) allowed for attack at the β site to be measured.

4.1 Room temperature OH kinetics

At room temperature under pseudo-first-order conditions ([OH] < 3 × 10^{12} molecule cm^{-3}, [n-butanol] > 1.5 × 10^{14} molecule cm^{-3}), the OH loss traces recovered from the first detection axis from the jet expanded gas corresponded closely with single exponential decays. These decays relate to the overall loss process for the reaction of OH with n-butanol:

$$OH + n\text{-}C_4H_9OH \rightarrow H_2O + \text{isomers of } C_4H_9O \qquad (R1)$$

The resulting rate coefficients were plotted against the concentration of butanol, in the presence of both low and high oxygen, as shown in Figure 9 (low oxygen < 5 × 10^{15} molecule cm^{-3}, high oxygen 1.2 × 10^{19} molecule cm^{-3}), where $k_{obs} = k_1 \times$ [butanol], giving a resultant bimolecular removal rate of $k_1 = (9.24 \pm 0.40) \times 10^{-12}$ cm^3 $molecule^{-1}$ s^{-1} under low oxygen conditions, and $k_1 = (9.23 \pm 0.15) \times 10^{-12}$ cm^3 $molecule^{-1}$ s^{-1} under high oxygen conditions.

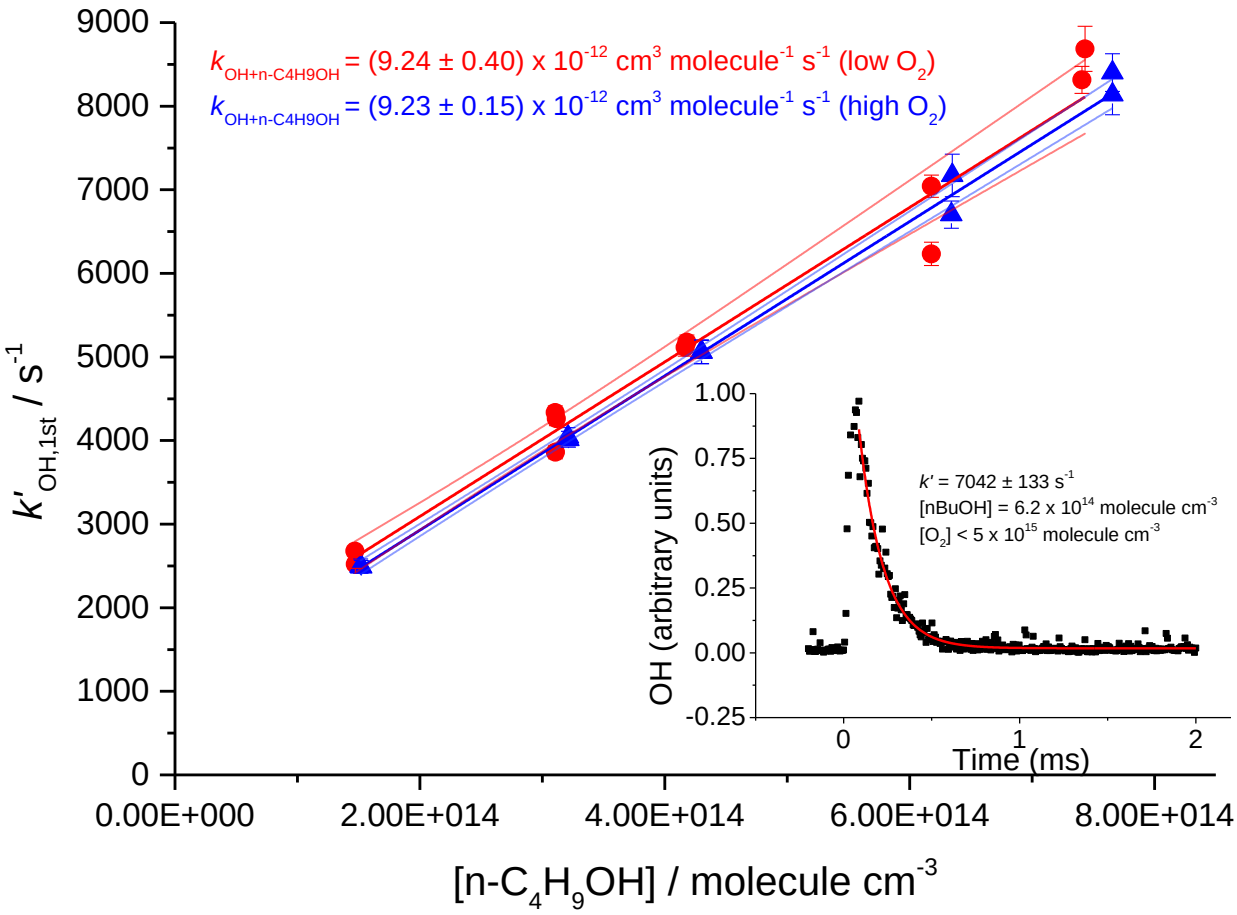

Figure 9. Plots $k'_{OH,1st}$ against the concentration of butanol, at two oxygen concentrations, < 5 × 10^{15} molecule cm^{-3} and 1.2 × 10^{19} molecule cm^{-3}. Bimolecular rate coefficients were taken from the slopes as $(9.24 \pm 0.40) \times 10^{-12}$ cm^3 $molecule^{-1}$ s^{-1} under low oxygen conditions (red circles with 95 % confidence limits), and $(9.23 \pm 0.15) \times 10^{-12}$ cm^3 $molecule^{-1}$ s^{-1} under high oxygen conditions (blue triangles with 95 % confidence limits). The inset shows a typical OH temporal profile at the first detection axis.

The good agreement between the measured rate coefficients with varying [O_2] verifies that, as expected under our experimental conditions at room temperature, the R radical formed from the β abstraction does not undergo fragmentation to OH and but-1-ene. The resultant combined data gives an overall 293 K bimolecular rate coefficient for OH and n-butanol of $k_1 = (9.24 \pm 0.21) \times$

10^{-12} cm^3 molecule^{-1} s^{-1}, which is in excellent agreement with the recent work of McGillen et al. (2013) of $k_{1,296}$ = (9.68 ± 0.75) × 10^{-12} cm^3 molecule^{-1} s^{-1}.

4.2 Room temperature HO_2 results

Experiments were carried out in high oxygen conditions (3 × 10^{17} – 1.2 × 10^{18} molecule cm^{-3}), at 296 – 303 K, and high pressures (1800 – 2000 Torr) of N_2 bath gas using photolysis of hydrogen peroxide at two different wavelengths (248 nm and 266 nm), and the resulting HO_2 yields are shown in Table 2. The resulting HO_2 yield was determined to be (58 ± 7) % at 266 nm, and (55 ± 12) % at 248 nm. As there is no significant variation in the yield with laser wavelength or power, we can treat the data in Table 2 as 12 independent estimates of the yield, giving an averaged HO_2 yield of 57% with a standard error (95%) of 6%. Therefore under the experimental conditions (pressure >1800 Torr, [O_2] > 3 × 10^{17} molecule cm^{-3}), the HO_2 yield, which originates from OH attack at the α abstraction site, was (57 ± 6) %, with a minor contribution from abstraction from the hydroxyl group. The yield assigned is in good agreement with McGillen et al. (2013) 57%, and Cavalli et al. (2002) 52 ± 7 %.

Table 2. HO_2 yields from experiments carried out at room temperature (293 – 298 K) with reaction initiated by photolysis of H_2O_2 at 248 nm and 266 nm.

Laser wavelength/nm	HO_2 Yield (%)							Average HO_2 Yield (%)
	Expt 1	Expt 2	Expt 3	Expt 4	Expt 5	Expt 6	Expt 7	
266	61 ± 7	54 ± 4	46 ± 5	56 ± 7	54 ± 7	67 ± 10	66 ± 6	58 ± 7
248	63 ± 2	68 ± 2	48 ± 5	52 ± 5	49 ± 5			55 ± 12

Experiments were carried out with photolysis at 266 nm and at a variety of laser energies at 248 nm, the yields remained consistent with photolysis wavelength and power. Varying the laser power did alter the profiles of the HO_2 traces recovered; the growth rates remained unaffected but the tails changed; decreasing laser power slowed the removal rate of HO_2 (from greater than 100 s^{-1} to under 10 s^{-1}) showing that radical-radical processes are the main source of HO_2 loss from the

system. If radical-radical reactions were an important source of any observed HO_2 yield changing laser power would have altered the HO_2 yield and additionally the HO_2 growth kinetics.

4.3 Higher temperature – HO_2 yield and OH recycling

The R radical formed from abstraction at the β site ($CH_3CH_2CHCH_2OH$) can regenerate OH and form butene, Scheme 2, in the absence of added oxygen. This process was not observed at ambient temperatures (293 – 305 K) but at elevated temperatures, 616 K – 657 K, the OH loss observed at the first detection axis was no longer well described by a single exponential loss process, Figure 10. The non-exponential decays formed were due to OH being returned following decomposition of the β R radical. Biexponential fits to the recycling traces gave the fraction of OH returned (Medeiros et al. 2018), with an average β branching fraction of (23 ± 4)%, Table 3.

Table 3. OH recycling and HO_2 yields from experiments carried out under elevated temperatures (> 600 K) all experiments were carried out with photolysis at 248 nm.

Temperature (K)	Fraction of OH returned (%)	Observed HO_2 Yield (%)
616	24.2 ± 4.1	54 ± 4
622	24.4 ± 4.9	
636	25.7 ± 5.6	
657	18.1 ± 4.0	

The HO_2 yield measured at an elevated temperature (616 K), where OH recycling was also observed, was 54 ± 4 % (Table 3) which is within error of the value (57 ± 6 %) measured at room temperature (293 K), although it is not possible to partition the HO_2 yield between α and OH abstraction. Over the temperature range tested the branching ratio for OH attack at the α position is therefore also likely to remain unchanged. With the sum of the α and β sites contributing (78 ± 4)%, at 616 K, the remainder of the abstraction (~22%) occurs at the δ and γ sites. These results are in excellent agreement of the product study of Cavalli et al. (2002) which found (52 ± 7)% α from the butanal product yield and (23 ± 4) % β from the propanal yield using FTIR detection and the site specific analysis by McGillen et al. (57 % α and 26% β). The product study of Hurley et al. (2009) found 44 ± 4 % α and 19 ± 2 % β values which are lower than our experimental values

but are within the combined error ranges. However, it should be noted that the β branching fraction of 23 ± 4 % measured in this study was obtained at elevated temperatures, 616 – 657 K.

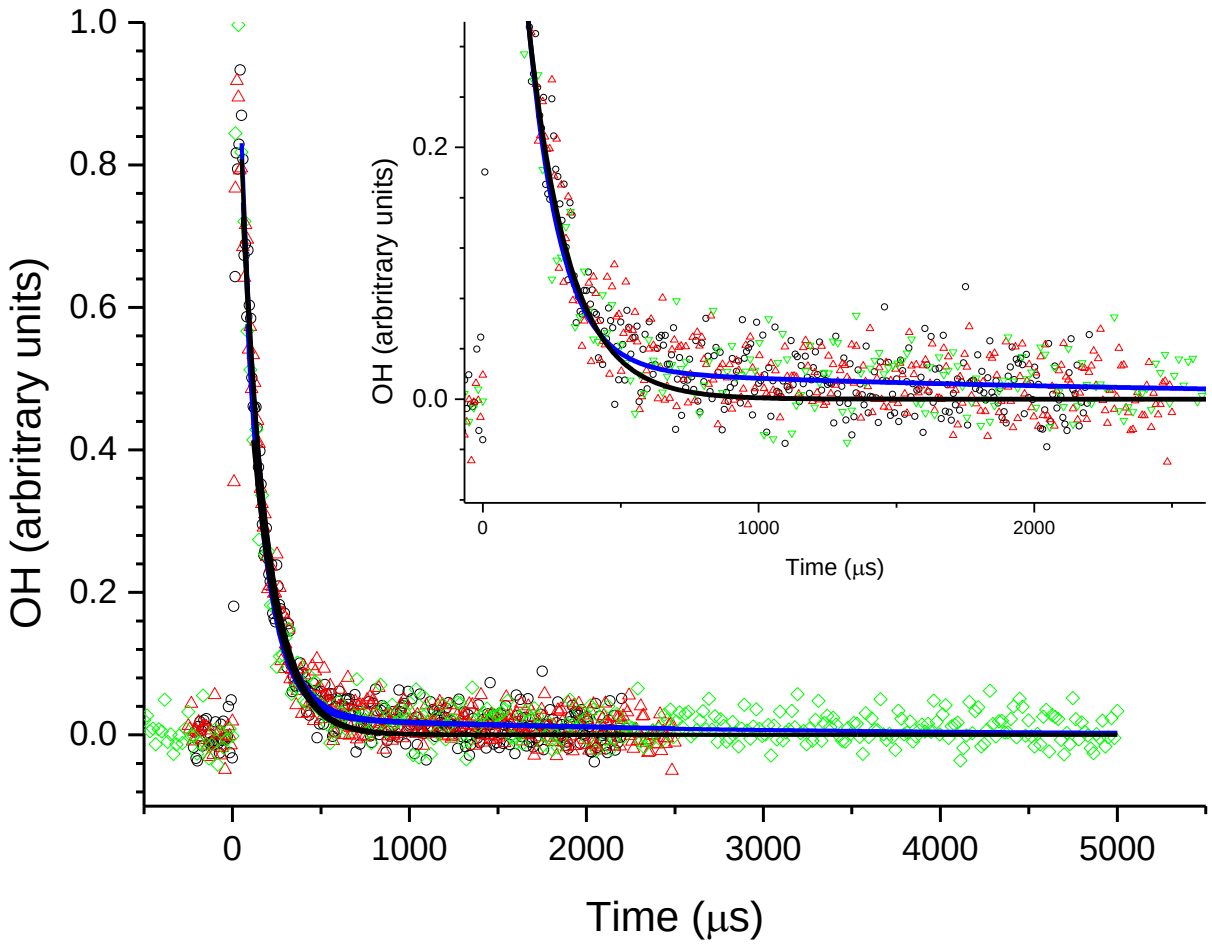

Figure 10. An example of the OH signal collected at the first detection axis for the reaction of OH with n-butanol ([nBuOH] ≈ 1.4 × 10^{15} molecule cm^{-3}, at 616 K, black, red and green points were three consecutive decays collected with differing timescales. The black line represents the least squares fits to an exponential decay ($k'_{1,1st}$ = (6780 ± 380) s^{-1}), with the blue line representing a bi-exponential fit ($k_{1,biexp,1st}$ = (8190 ± 180) s^{-1})). Both lines are global fits to the three experiments.

5 Summary

An instrument based on the FAGE technique for monitoring OH radicals and validated via reproduction of the literature kinetics of several OH reactions over a wide range of temperatures

and pressures, has been extended to allow for simultaneous HO_2 and OH detection via the chemical titration of HO_2 to OH with NO.

As mentioned in the introduction, the instrument has similarities to that presented by Nehr et al. (2011), where a FAGE system for sequential OH and HO_2 is coupled to a lifetime instrument and yields of HO_2 from OH initiated reactions are reported. Although the principles of HOx detection used in both systems is similar, there are some significant differences between the two instruments. Some differences relate to the reaction cell in which the kinetics takes place: 1 atm of air and 298 K for Nehr et al. and 0.5 – 5 atm of any gas and 298 – 800 K for this work. However, in principle, the Nehr et al. FAGE cell could be coupled to a different reaction cell to probe a wider range of conditions. A more substantial difference is the timescale of the chemistry taking place. Typical temporal profiles from Nehr et al. are of the order of a second compared to <10 ms in this work. The enhanced sensitivity of the Nehr et al. instrument means that radical-radical reactions should not interfere, but the technique may be subject to interferences from first order (or pseudo-first order) reactions including heterogeneous processes. Detection of radicals in kinetics or yield experiments is difficult and studying reactions under a range of conditions is important to identify systematic errors, hence both instruments have a role to play.

The use of H_2O_2 as an OH precursor has been shown to provide a reliable method of internally characterizing our system for HO_2 yield detection. Interferences that could arise from using this precursor for HO_2 detection have been accounted for, and the presence of water that the H_2O_2 precursor introduces has no effect on the sensitivity of the LIF method, unlike IR absorption methods.

It has been demonstrated that this instrument can reliably assign HO_2 yields and simultaneously measure OH kinetics, even under conditions of high temperatures and high oxygen concentrations, which could be challenging for other detection systems. Such conditions are important for exploring key combustion chemistry reactions, and for converting slow atmospherically relevant processes to the microsecond timescales required to minimize secondary or heterogeneous chemistry.

By performing reactions under low NOx and low radical densities ($<1\times10^{13}$ molecule cm^{-3}), HO_2 yields formed on fast timescales (> 300 s^{-1}) can be assigned to direct HO_2 channels or reactions of alkyl (R) radicals with oxygen. Whilst some time-resolution is lost at the HO_2 detector,

sufficient time-resolution is retained in order to separate varying sources of HO_2, for example the two channels leading to HO_2 production in the $OH/CH_3OH/O_2$ system (Section 3.2) or from unwanted secondary chemistry.

For particular reactions, illustrated in this paper by the study of OH with methanol and butanol in the presence of oxygen, the simultaneous measurement of OH kinetics and HO_2 yields can provide important site-specific information. In other systems, the onset of HO_2 formation could allow for the assignment of new channels becoming important within complex mechanism, potentially allowing for verifying the onset of OOQOOH chemistry within OH regeneration processes.

6 Acknowledgements

A studentship from NERC through the University of Leeds 'Spheres' Doctoral Training Programme for T.H. Speak is gratefully acknowledged.

7 Author Contributions

THS undertook most of the experimental measurements and contributed to the first draft of the manuscript. DS provided input into experimental design and analysis of transport effects. MAB and PWS lead the project and completed the manuscript.

8 Competing Interests

The authors declare that they have no conflicts of interest.

9 References

Agbro, E., Tomlin, A. S., Lawes, M., Park, S., and Sarathy, S. M.: The influence of n-butanol blending on the ignition delay times of gasoline and its surrogates at high pressures, Fuel, 187, 211-219, 10.1016/j.fuel.201609.052, 2017.

Assaf, E., and Fittschen, C.: Cross Section of OH Radical Overtone Transition near 7028 cm^{-1} and Measurement of the Rate Constant of the Reaction of OH with HO_2 Radicals, J. Phys. Chem. A, 120, 7051-7059, 10.1021/acs.jpca.6b06477, 2016.

Assaf, E., Liu, L., Schoemaecker, C., and Fittschen, C.: Absorption spectrum and absorption cross sections of the $2v_1$ band of HO_2 between 20 and 760 Torr air in the range 6636 and 6639 cm^{-1}, J. Quant. Spectrosc. Radiat. Transfer, 211, 107-114, 10.1016/j.jqsrt.2018.02.035, 2018.

Atkinson, R., Aschmann, S. M., Winer, A. M., and Pitts, J. N.: Rate constants for the reaction of OH radicals with a series of alkanes and alkenes at 299 +/- 2 K, Int. J. Chem. Kinet., 14, 507-516, 10.1002/kin.550140508, 1982.

Atkinson, R., Baulch, D. L., Cox, R. A., Crowley, J. N., Hampson, R. F., Hynes, R. G., Jenkin, M. E., Rossi, M. J., and Troe, J.: Evaluated kinetic and photochemical data for atmospheric chemistry: Volume II - gas phase reactions of organic species, Atmos. Chem. Phys., 6, 3625-4055, 2006.

Baeza-Romero, M. T., Blitz, M. A., Goddard, A., and Seakins, P. W.: Time-of-flight mass spectrometry for time-resolved measurements: Some developments and applications, Int. J. Chem. Kinet., 44, 532-545, 10.1002/kin.20620, 2012.

Brune, W. H., Stevens, P. S., and Mather, J. H.: Measuring OH and HO_2 in the troposphere by laser-induced fluorescence at low-pressure, J. Atmos. Sci., 52, 3328-3336, 10.1175/1520-0469(1995)052<3328:moahit>2.0.co;2, 1995.

Cavalli, F., Geiger, H., Barnes, I., and Becker, K. H.: FTIR kinetic, product, and modeling study of the OH-initiated oxidation of 1-butanol in air, Environmental Science & Technology, 36, 1263-1270, 10.1021/es010220s, 2002.

Crowley, J. N., Simon, F. G., Burrows, J. P., Moortgat, G. K., Jenkin, M. E., and Cox, R. A.: The HO_2 radical UV absorption-spectrum measured by molecular modulation, UV diode-array spectroscopy, Journal of Photochemistry and Photobiology A-Chemistry, 60, 1-10, 10.1016/1010-6030(91)90001-a, 1991.

Dunlop, J. R., and Tully, F. P.: A kinetic study of OH radical reactions with methane and perdeuterated methane, J. Phys. Chem., 97, 11148-11150, 10.1021/j100145a003, 1993.

Edwards, G. D., Cantrell, C. A., Stephens, S., Hill, B., Goyea, O., Shetter, R. E., Mauldin, R. L., Kosciuch, E., Tanner, D. J., and Eisele, F. L.: Chemical ionization mass spectrometer instrument for the measurement of tropospheric HO_2 and RO_2, Anal. Chem., 75, 5317-5327, 10.1021/ac034402b, 2003.

Fuchs, H., Bohn, B., Hofzumahaus, A., Holland, F., Lu, K. D., Nehr, S., Rohrer, F., and Wahner, A.: Detection of HO_2 by laser-induced fluorescence: calibration and interferences from RO_2 radicals, Atmos. Meas. Tech., 4, 1209-1225, 10.5194/amt-4-1209-2011, 2011.

Gianella, M., Reuter, S., Aguila, A. L., Ritchie, G. A. D., and van Helden, J. P. H.: Detection of HO_2 in an atmospheric pressure plasma jet using optical feedback cavity-enhanced absorption spectroscopy, New Journal of Physics, 18, 10.1088/1367-2630/18/11/113027, 2016.

Glowacki, D. R., Goddard, A., Hemavibool, K., Malkin, T. L., Commane, R., Anderson, F., Bloss, W. J., Heard, D. E., Ingham, T., Pilling, M. J., and Seakins, P. W.: Design of and initial results from a highly instrumented reactor for atmospheric chemistry (HIRAC), Atmos. Chem. Phys., 7, 5371-5390, 2007.

Hanke, M., Uecker, J., Reiner, T., and Arnold, F.: Atmospheric peroxy radicals: ROXMAS, a new mass-spectrometric methodology for speciated measurements of HO_2 and ΣRO_2 and first results, International Journal of Mass Spectrometry, 213, 91-99, 10.1016/s1387-3806(01)00548-6, 2002.

Hard, T. M., O'Brien, R. J., Chan, C. Y., and Mehrabzadeh, A. A.: Tropospheric Free-radical determination by FAGE, Environmental Science & Technology, 18, 768-777, 1984.

Hurley, M. D., Wallington, T. J., Lauirsen, L., Javadi, M. S., Nielsen, O. J., Yamanaka, T., and Kawasaki, M.: Atmospheric Chemistry of n-Butanol: Kinetics, Mechanisms, and Products of Cl Atom and OH Radical Initiated Oxidation in the Presence and Absence of NOx, J. Phys. Chem. A, 113, 7011-7020, 10.1021/jp810585c, 2009.

Jemialade, A. A., and Thrush, B. A.: Reactions of HO_2 with NO and NO_2 studied by midinfrared laser magnetic-resonance, Journal of the Chemical Society-Faraday Transactions, 86, 3355-3363, 10.1039/ft9908603355, 1990.

McCaulley, J. A., Kelly, N., Golde, M. F., and Kaufman, F.: Kinetic studies of the reactions of F and OH with CH_3OH, J. Phys. Chem., 93, 1014-1018, 10.1021/j100340a002, 1989.

McGillen, M. R., Baasandorj, M., and Burkholder, J. B.: Gas-Phase Rate Coefficients for the OH plus n-, i-, s-, and t-Butanol Reactions Measured Between 220 and 380 K: Non-Arrhenius Behavior and Site-Specific Reactivity, J. Phys. Chem. A, 117, 4636-4656, 10.1021/jp402702u, 2013.

Medeiros, D. J., Blitz, M. A., James, L., Speak, T. H., and Seakins, P. W.: Kinetics of the Reaction of OH with Isoprene over a Wide Range of Temperature and Pressure Including Direct Observation of Equilibrium with the OH Adducts, J. Phys. Chem. A, 122, 7239-7255, 10.1021/acs.jpca.8b04829, 2018.

Monks, P. S.: Gas-phase radical chemistry in the troposphere, Chemical Society Reviews, 34, 376-395, 10.1039/B307982C, 2005.

Moore, S. B., and Carr, R. W.: Molecular velocity distribution effects in kinetic studies by time-resolved mass-spectrometry, Int. J. Mass Spectrom. Ion Processes, 24, 161-171, 10.1016/0020-7381(77)80023-5, 1977.

Nehr, S., Bohn, B., Fuchs, H., Hofzumahaus, A., and Wahner, A.: HO_2 formation from the OH plus benzene reaction in the presence of O_2, Phys. Chem. Chem. Phys., 13, 10699-10708, 10.1039/c1cp20334g, 2011.

Onel, L., Brennan, A., Gianella, M., Ronnie, G., Aguila, A. L., Hancock, G., Whalley, L., Seakins, P. W., Ritchie, G. A. D., and Heard, D. E.: An intercomparison of HO_2 measurements by fluorescence assay by gas expansion and cavity ring-down spectroscopy within HIRAC (Highly Instrumented Reactor for Atmospheric Chemistry), Atmos. Meas. Tech., 10, 4877-4894, 10.5194/amt-10-4877-2017, 2017.

Orlando, J. J., Tyndall, G. S., Bilde, M., Ferronato, C., Wallington, T. J., Vereecken, L., and Peeters, J.: Laboratory and theoretical study of the oxy radicals in the OH- and Cl-initiated oxidation of ethene, J. Phys. Chem. A, 102, 8116-8123, 10.1021/jp981937d, 1998.

Orlando, J. J., Tyndall, G. S., and Wallington, T. J.: The atmospheric chemistry of alkoxy radicals, Chemical Reviews, 103, 4657-4689, 2003.

Reitz, R. D., and Duraisamy, G.: Review of high efficiency and clean reactivity controlled compression ignition (RCCI) combustion in internal combustion engines, Progress in Energy and Combustion Science, 46, 12-71, 10.1016/j.pecs.2014.05.003, 2015.

Stockwell, W. R., Lawson, C. V., Saunders, E., and Goliff, W. S.: A Review of Tropospheric Atmospheric Chemistry and Gas-Phase Chemical Mechanisms for Air Quality Modeling, Atmosphere, 3, 1, 2012.

Stone, D., Whalley, L. K., and Heard, D. E.: Tropospheric OH and HO_2 radicals: field measurements and model comparisons, Chem. Soc. Rev., 41, 6348-6404, 10.1039/c2cs35140d, 2012.

Stone, D., Blitz, M., Ingham, T., Onel, L., Medeiros, D. J., and Seakins, P. W.: An instrument to measure fast gas phase radical kinetics at high temperatures and pressures, Review of Scientific Instruments, 87, 054102, 2016.

Taatjes, C. A., and Oh, D. B.: Time-resolved wavelength modulation spectroscopy measurements of HO_2 kinetics, Appl. Opt., 36, 5817-5821, 10.1364/ao.36.005817, 1997.

Taatjes, C. A.: How does the molecular velocity distribution affect kinetics measurements by time-resolved mass spectrometry?, Int. J. Chem. Kinet., 39, 565-570, 10.1002/kin.20262, 2007.

Thiebaud, J., and Fittschen, C.: Near infrared cw-CRDS coupled to laser photolysis: Spectroscopy and kinetics of the HO_2 radical, Appl. Phys. B-Lasers Opt., 85, 383-389, 10.1007/s00340-006-2304-0, 2006.

Tully, F. P.: Laser photolysis laser-induced fluorescence study of the reaction of hydroxyl radical with ethylene, Chem. Phys. Lett., 96, 148-153, 10.1016/0009-2614(83)80481-3, 1983.

Whalley, L. K., Blitz, M. A., Desservettaz, M., Seakins, P. W., and Heard, D. E.: Reporting the sensitivity of laser-induced fluorescence instruments used for HO_2 detection to an interference from RO_2 radicals and

introducing a novel approach that enables HO_2 and certain RO_2 types to be selectively measured, Atmos. Meas. Tech., 6, 3425-3440, 10.5194/amt-6-3425-2013, 2013.

Wine, P. H., Semmes, D. H., and Ravishankara, A. R.: A laser flash-photolysis kinetics study of the reaction $OH+H_2O_2 = HO_2+H_2O$, J. Chem. Phys., 75, 4390-4395, 10.1063/1.442602, 1981.

Winiberg, F. A. F., Smith, S. C., Bejan, I., Brumby, C. A., Ingham, T., Malkin, T. L., Orr, S. C., Heard, D. E., and Seakins, P. W.: Pressure-dependent calibration of the OH and HO_2 channels of a FAGE HOx instrument using the Highly Instrumented Reactor for Atmospheric Chemistry (HIRAC), Atmos. Meas. Tech., 8, 523-540, 10.5194/amt-8-523-2015, 2015.

Zador, J., Taatjes, C. A., and Fernandes, R. X.: Kinetics of elementary reactions in low-temperature autoignition chemistry, Progress in Energy and Combustion Science, 37, 371-421, 10.1016/j.pecs.2010.06.006, 2011.

REVIEWER 1 RESPONSES

First comment 1:

"However, I have, besides some minor remarks, a major concern: you do not take into account any secondary radical-radical reaction with the argument, that your radical concentrations are low enough. I do not agree with this point, even though it is not always easy to get enough details from the manuscript to judge. So my comment is based on your statement page 6, that the typical initial OH concentration is between 2e11 and 5e13 cm-3. In the below graph are shown two simulations with [OH]0 = 1e12 and H2O2 = 5e14 (left) and [OH]0 = 1e13 and [H2O2] = 1e15 (right graph). The blue symbols show the simple model OH + H2O2 ◊ HO2 + H2O, while the green symbols include on top the reaction of OH + HO2 ◊ H2O + O2 with 1e-10 cm3 s -1 . t / s [OH, HO2] 0.000 0.002 0.004 0.006 0.008 0.010 0 5.0×101 1 1.0×101 2 HO2 OH with secondary reactions OH w/o secondary reactions Y0 Plateau K oh 1.001e+012 = 0.0 887.4 x 10.000e+011 = 0.0 848.7 HO2_ini k_slow HO2_sec k_fast ho2 = 0.0 3.015 8.923e+011 949.9 xy = 0.0 -0.03680 9.998e+011 849.2 HO2 t / s [OH, HO2] 0.000 0.001 0.002 0.003 0.004 0.005 0 5.0×101 2 1.0×101 3 Y0 Plateau K oh 1.002e+013 = 0.0 2003 x 9.998e+012 = 0.0 1687 HO2_ini k_slow HO2_sec k_fast ho2 = 0.0 20.16 6.379e+012 2596 xy = 0.0 -0.09674 9.993e+012 1691 ho2 oh x It can very clearly be seen that even under the relatively low initial radical concentration of 1e12 (which is at your lower end) already the HO2 yield is not 100% anymore, situation gets much worse with 1e13 OH: only 60% of the initial OH is converted to HO2. This has also an influence on the OH decay rate, as well as on the retrieved HO2 rise time (both get faster). This "problem" has been discussed in detail by Assaf et al, JPCA 2016, when using this system to retrieve the OH absorption cross section. In your case not taking into account secondary chemistry will lead to an overestimation of the HO2 yield.

Of course taking into account this chemistry is possibly only if you know the absolute initial OH concentration. Maybe you did some experiments were you varied the photolysis energy? Because this would give you an idea if secondary reactions are important or not under your conditions. In the case of the OH + CH3OH experiments, secondary chemistry might play a role as well. Very recently, Assaf et al (PCCP, 20, 10660, 2018) have measured the rate constant of CH3O + HO2 and CH3O + CH3O, both have found to be very fast (1.1e-10 and 7e-11 cm3 s -1). The result is that even under moderate high initial radical concentrations, some CH3O will react away before it is converted into HO2. You find a yield in good agreement with literature, either your initial radical concentration are at the lower end of the indicated range, or maybe the internal calibration, tending to overestimate the yield, makes up for this underestimation. Please give more information on the estimated initial radical concentration for the different experiments and check, if your systems are really free from secondary chemistry. In any case, before I can agree to the sentence that your instrument can accurately measure HO2 yields, I would like to see a more detailed discussion on possible secondary chemistry."

Response

Thank you for this very pertinent question. Prior to submission many checks for radical-radical effects were made by varying the repetition rate and photolysis laser power, and no observed differences were seen in the HO_2 yields. We had based our statement on the empirical observations rather than a review of the possible secondary chemistry, however, your careful review and analysis, does suggest that we ought to see a significant difference. The literature does imply we should see a change in HO_2 yield between OH + H_2O_2 and OH + CH_3OH/O_2 (n.b. note that the same high [O_2]

is used in both experiments. As the [OH] is increased we should get an ~50 % yield when [OH] ~= 3E13 cm^{-3} and OH + H_2O_2 is used as the OH → HO_2 conversion reaction. Also the observed OH removal kinetics of the OH + H_2O_2 reaction should increase with [OH]; >20% faster when [OH] ~=3E13 cm^{-3}. Because of this inconsistency of our result with the literature, we have carried a number of new experiments, where the [OH] is varied over a greater range, varying pump laser power from 0.5-60 mJ cm^{-2}. The take home message is that we cannot reproduce the literature, and our HO_2 yields / kinetics for the reaction OH + H_2O_2 are close to unchanged over all [OH] from 2E11 up to 5E13 molecule cm^{-3}.

We are in agreement with the reviewer as to the implications of the literature. From a model (as detailed by the reviewer), when [OH]0 = 1E13 cm^3, the HO_2 yield from OH + H_2O_2 is about 50% compared to when a large excess of methanol is added, see Fig 1.

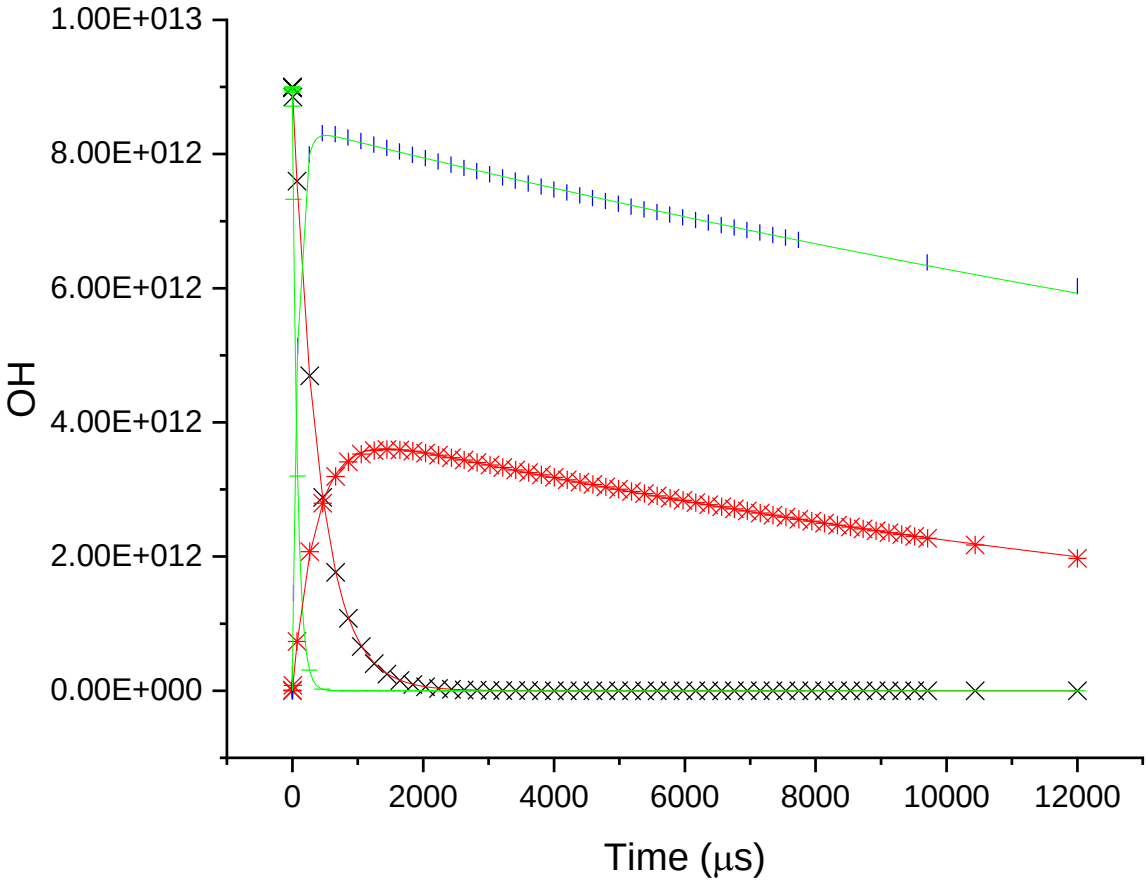

Figure 1 A simulation of the expected HO_2 yields for reaction of 9E12 OH with 1E15 H_2O_2 with 6E18 O_2, in the presence and absence of 1E16 methanol. Where the removal of OH by reaction with the HO_2, OH were included, and accounting for the loss of HO_2 via reaction with HO_2, OH, CH_3O and diffusion.

The crucial reaction in attenuating the HO_2 yield in the OH + H_2O_2 reaction is OH + HO_2. According to the literature the HO_2 yield will only be close to unity when [OH] < 1E12 cm^{-3}. Also, it

is noted that when OH + HO_2 is significantly occurring the OH + H_2O_2 kinetics will be significantly faster than the literature. Based on these predictions we have done further experiments.

Also note that by comparing HO_2 yield when $CH_3OH(O_2)$ is present we can assign yields without knowing the absolute radical concentration; it is wholly reasonable to assign the HO_2 yield in the presence of sufficient $CH_3OH(O_2)$ as100%.

The literature predicts a large decrease in the HO_2 yield from hydrogen peroxide as the $[OH]_0$ is increased, see Fig 1. Below is our yield for HO_2 from OH + H_2O_2 and is compared to when a large amount of $CH_3OH(O_2)$ is added. It is clear that no attenuation of the HO_2 yield is observed in our system. Many other experiments were carried out as $[OH]_0$ was varied over a factor of ~300, and the HO_2 yield from all the experiments was the same, within error, for OH + H_2O_2 compared to when $CH_3OH(O_2)$ is added. The $[H_2O]$ and $[CH_3OH]$ in the system is too small for significant complexation to HO_2. Our experiments assign yields as 100% (99 ± 7 at 1E11 [OH], 99 ± 2 at 3E12 [OH] and 98 ± 3 at 3E13 [OH]).

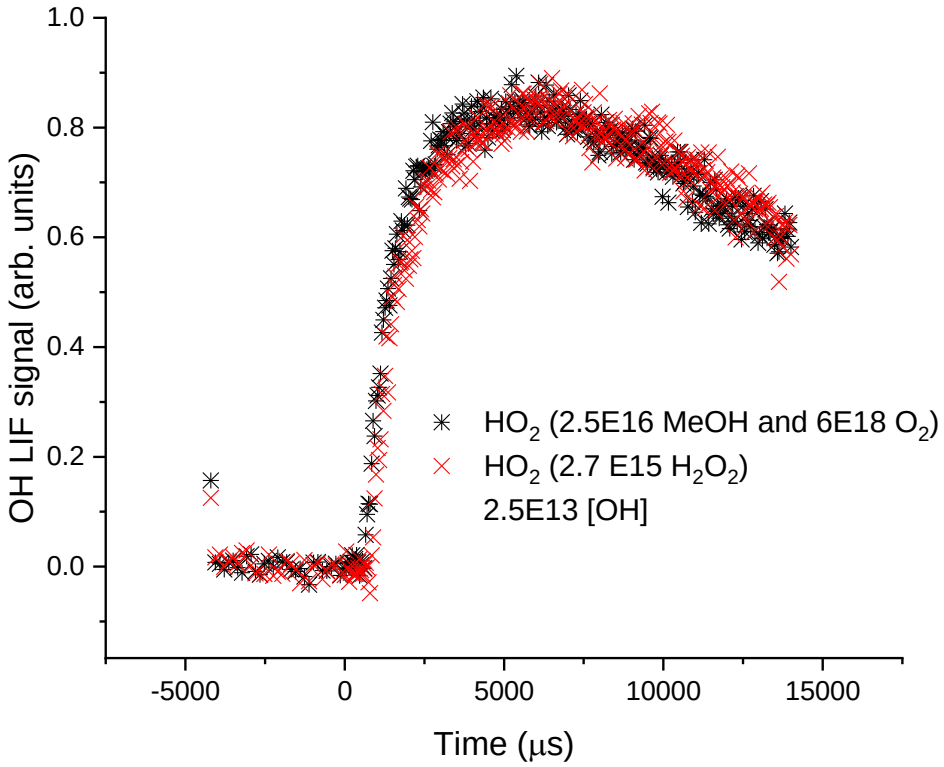

Figure 2 HO_2 growth profiles collected with 2.5E13 cm^{-3} [OH], 6E18 cm^{-3} O_2, 2.7E15 H_2O_2 in the presence and absence of 2.5E16 CH_3OH.

Also, the impact of the HO_2 + OH on the observed OH + H_2O_2 rate constant is to make it significantly faster as the initial [OH] is increased. From our literature model, measurable changes in the rate constant should be observed as [OH] is increased >20 % for 1 Hz experiments; in experiments carried out at 10 Hz where there is HO_2 present from the previous laser flash at time zero, this should lead to the observation of an increase in the OH removal rate by up to 50 %. The precision of the system means that we can readily see changes in the rate constant to ~ 1%. The results are summarised is the graph below.

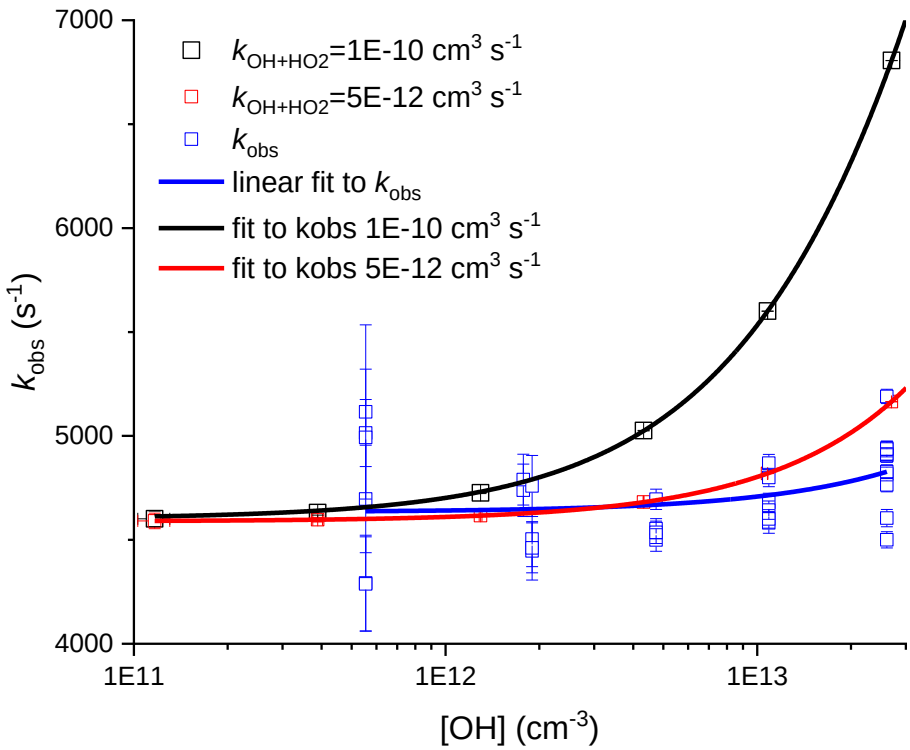

Figure 3 Expected and observed OH removal rates with 2.7E15 cm^{-3} H_2O_2 and 1-60 mJ cm^{-2} photolysis energy at 248 nm and 10Hz.

Again, this kinetics test versus [OH] demonstrates that under our conditions HO_2 + OH is having little impact on the OH + H_2O_2 reaction. The measurable increase in the figure 3 (6.8%) can be assigned to OH + OH (=1E-11 cm^3 s^{-1}, at 1600 Torr).

We recognise that our results are in contradiction with the literature rate coefficient for HO_2 + OH. The IUPAC literature value is 1.1E-10 cm^3 s^{-1}. In order to reconcile our experiments we require this rate coefficient to be < 1E-11 cm^3 s^{-1}. However, our result is wholly consistent with the previous paper on the reaction of OH with H_2O_2 (Wine et al. 1981 J. Chem. Phys). In Wine et al. the removal kinetics were not perturbed by additional HO_2 added to the system. In this work, with additional [HO_2] ~ 1E13 added, no measurable change in the OH + H_2O_2 was observed. This result is in agreement with our present study. We note that Wine et al study used flash photolysis study, as used in our present study. Most literature assignments on HO + HO_2 were carried out in low pressure, flow tubes; very different conditions. The flash photolysis is less prone to interference.

We have added new material in the provisional revised manuscript, **lines 382 – 396**.

'A possible interference that could distort the yield of HO_2 is the role of the radical-radical reaction OH + HO_2 (Assaf and Fittschen, 2016):

$OH + HO_2 \rightarrow H_2O + O_2$ $\quad k_{15} = 1.1 \times 10^{-10}$ cm^3 molecule^{-1} s^{-1} Atkinson et al. (2006) (R15)

At the low radical concentrations used in many experiments in this work, this reaction could contribute 5 – 10% of the OH loss in an OH + H_2O_2 calibration experiment. However, we have looked at the dependence of the HO_2 yield from both OH/H_2O_2 and from OH/CH_3OH, but see no significant effects of secondary radical-radical reaction (<5%) as the calculated $[OH]_0$ is changed from 5×10^{11} to 5×10^{12} molecule cm^{-3}. For the OH/CH_3OH the much larger concentrations of substrate used lead to faster pseudo-first order decays, so radical-radical contribution is significantly reduced. The work of Assaf and Fittschen suggests that a more significant deviation in the OH loss rates, and one that we ought to be to detect given the precision of our data, should be observed. It is possible that our calculations of $[OH]_0$ are over-estimated, but we note that a study of the OH + H_2O_2 reaction by Wine et al. (1981), where they specifically looked for the interference on OH decays from R15, could find no evidence for an increase in the loss of OH, when $[HO_2]$ was artificially increased.'

Comment 2:

"Figure 3 : the black squares are difficult to distinguish from the blue triangle. Better chose other symbols or other colours."

Response:

In part, that these are hard to distinguish is due to these traces showing no evidence of back diffusion of NO into the region where the OH is probed in the first detection axis. We have tried to improve figures by using open symbols in cases.

Comment 3:

"Figure 7: Who is who? I guess red is HO2 and black is OH? What was the reaction system in Figure 7 and what was the estimated initial radical concentration? Because from the above model, one would expect a faster HO2 decay compared to OH decay if secondary reactions are taken into account (2003 s -1 for OH against 2596 s-1 for HO2 in the example of the right graph above)."

A legend has been provided in the revised manuscript and the OH concentrations were 1-3 E12 cm^{-3}. The experimental detail has now been included in the description.

Please see the response above for comment on observations of secondary reactions.

Comment 4:

Figure 10: what are the different colored symbols? Different experiments? Or is the blue line a fit to different data points?

Response:

The red fit is an exponential fit to the data, the blue fit is a multi-exponential fit that allows for assignment of the returned OH. The three colours of symbols are merely three different time scans of the same experimental conditions to allow for correct assignment of both the fast and slow loss processes. **Additional material in the caption has added clarity** to this figure.

REVIEWER 2 RESPONSES

Atmos. Meas. Tech. Discuss., doi:10.5194/amt-2019-164-RC1, 2019 © Author(s) 2019. "A New Instrument for Time Resolved Measurement of HO2 Radicals" by Thomas H. Speak et al. Anonymous Referee #2

The authors describe an experimental apparatus to determine HO_2 yields and OH reaction kinetics in a pump-probe flow-tube experiment. The paper is suitable for publication in AMT after addressing the following points:

Comment 1:

P1 L19/20: As written now, the statement only verifies the OH kinetics.

"As an application of the new instrument, the reaction of OH with n-butanol has been studied at 293 and 616 K. The bimolecular rate coefficient at 293 K, $(9.24 \pm 0.21) \times 10^{-12}$ cm^3 $molecule^{-1}$ s^{-1} (18 , 19) is in good agreement with recent literature, verifying that this instrument can both measure HO_2 yields and accurate OH kinetics."

Response:

Agreed, the wording is unclear and is now worded as (removing mention of yields):

'The bimolecular rate coefficient at 293 K, $(9.24 \pm 0.21) \times 10^{-12}$ cm^3 $molecule^{-1}$ s^{-1} is in good agreement with recent literature, verifying that this instrument can measure accurate OH kinetics.'

Validation of the HO_2 yields is emphasised later in the abstract, where we now state:

'Direct observation of the HO_2 product in the presence of oxygen has allowed the assignment of the α-branching fractions (0.57 ± 0.06) at 293 K and (0.54 ± 0.04) at 616 K), again in good agreement with the literature;'

Comment 2:

P2 L41/42: It would be useful to show the explicit reactions.

"whereas abstraction at other sites leads to alkylperoxy radical (C4H9O2)formation with varying fractions of the RO2 forming alkoxy radicals, and subsequently HO2 (McGillen et al., 2013) on a longer timescale."

Response:

The decision has been made to use Scheme 2 to provide clarity on these reactions (listing all reactions takes up too much space) and this has been moved to the relevant part of the manuscript.

Comment 3:

P6 L148: What was the repetition rate of the laser?

"The photolysis of the OH precursor, H2O2, at 248 nm (Lambda Physik, Compex 200 operated using KrF) or 266 nm (frequency quadrupled Nd-YAG output, Quantel, Q-smart 850) initiated the chemistry."

Response:

Experiments were carried out with repetition rates varied between 0.5 and 10 Hz, varying the repetition rates within this range did not affect the observed OH kinetics and HO_2 yields. As a result of this repetition rate independence, in general experiments were carried out at 5 Hz for 248 nm and 10 Hz for 266 nm. However, for each reaction the assumption of repetition rate independence was verified by performing an experiment at 1 Hz in addition to the higher repetition rate experiments.

An explicit description of this is now included. In addition, this will be discussed clearly in the description of the work done to check for the effect of any radical radical processes that will be included at the behest of Reviewer 1.

Revised wording (**line 155**):

'The photolysis of the OH precursor, H_2O_2, at 248 nm (Lambda Physik, Compex 200 operated using KrF at 1 or 5 Hz) or 266 nm (frequency quadrupled Nd-YAG output, Quantel, Q-smart 850 at 1 or 10 Hz) initiated the chemistry. No significant difference was noted in the kinetics or yields as a function of laser repetition rate.'

Comment 4:

P8 L182: Which range and which resolution was used for the delay between photolysis and detection?

Response:

Typical experimental traces contained 200 – 300 data points sampling the experimental time frame which were in the range 50 – 190,000 microseconds at 5 Hz, and 50 – 95,000 microseconds at 10 Hz. Typical delays between the pump and probe lasers were on the microsecond timescale with control of these timings in the high nanoseconds.

This is now described more clearly in the provisional revised manuscript (**line 189**). 'A delay generator (BNC DG535) was used to vary the delay (time resolution ~10 ns) between the photolysis and probe laser, facilitating generation of time profiles of the OH concentration. The traces, typically 200 – 300 data points and ranging in time from ~50 μs – 20 ms, were scanned through multiple times (5 – 20) and the signal at each time point was averaged, giving high precision OH loss traces.'

Comment 5:

P8 L201: Could the authors show here or elsewhere that the chemistry stopped, when the air entered the low-pressure cells or what the influence on the measurement was, if not?

Response:

The pressure drop (1600 – 0.5 Torr) from the high pressure to the low pressure cell will reduce the rate of bimolecular reactions proportionally. It is acknowledged that the density in the jet itself is higher (10 – 60 Torr). However, rate constants can be measured within 1-2 % of the literature (Medieros et al. *J. Phys. Chem. A* 2018), and minimal quenching of the OH LIF signal over a wide range of added oxygen show that chemistry occurring within the jet is minimal. For unimolecular reactions, the temperature change from the expansion ensures that the rates of these processes are slowed significantly.

Comment 6:

P11 L246-252: Could the authors give some numbers for the correction?

" For reactions carried out where a reagent was added in addition to the H2O2, the resulting ratios can be compared with those from the calibration reaction to allow assignment of an observed HO2 yield. To assign the HO2 yield from the test reaction required accounting for secondary HO2 production in the high-pressure reactor, from OH + H2O2 and photolysis processes. From the known rate coefficients, it was possible to calculate the fraction of OH reacting with the H2O2 and hence the expected contribution to the HO2 signal. Photolytic production of HO2 was accounted for by measuring the observed HO2 signal in the absence of any H2O2."

Response:

OH and RH was typically kept 10 to 20 times faster than OH and hydrogen peroxide and from this using the kinetics of the respective reactions the fraction of OH that reacted with the precursor could simply be accounted for. In general, this accounted for 5 to 10 % of the observed HO_2 signal and this is accounted for explicitly within our analysis.

Where photolysis of the reagents leads to HCO or H in the presence of oxygen this provides an additional source of HO_2. The observed signal in the absence of the OH precursor was subtracted from signal in the presence of the OH precursor. For the reactions included in this paper there was no observed photolysis of the reagents.

$RO_2 + RO_2$ can be a source of HO_2 however under our experimental conditions this forms too slowly (2-80 s^{-1}) to provide a significant increased HO_2 yield.

Revised text (**line 257**)

'From the known rate coefficients, it was possible to calculate the fraction of OH reacting with the H_2O_2 (typically 5 – 10%) and hence the expected contribution to the HO_2 signal.'

Comment 7:

P11 L253-268: The description could be extended by giving more details what exactly is calculated and how calibration numbers are derived. Is an absolute OH calibration of the cells needed for this approach? If so, how was this achieved?

Response:

No, absolute concentrations are not required. A reference reaction with a known HO_2 yield is used and then compared to the reaction under study, as stated in Lines 240 to 252 of the original manuscript.

1022 This has been validated by comparing two reference reactions OH and H_2O_2 and OH and CH_3OH with high
1023 oxygen, 100 % HO_2. By proving that H_2O_2 and CH_3OH give the same HO_2 yields we can simply use OH and
1024 H_2O_2 on its own.

1025 **Comment 8:**

1026 *P14 L346: What are the consequences for not so well-known systems? Is there a strategy how to*
1027 *estimate the RO2 fraction in the signal or at least to know, if RO2 influenced the yield?*

1028 "For test reagents which can generate radicals similar to hydroxyethylperoxy, our instrument will detect
1029 both HO2 and RO2 with some selectivity to HO2."

1030 **Response:**

1031 As with all FAGE HO_2 detectors this instrument will not fully discriminate between RO_2 and HO_2. As
1032 highlighted in this section the instrument cannot be described as exclusively an HO2 detector.

1033 Discriminating RO_2 from HO_2 relies on the requirement for multiple NO reactions for OH formation in the
1034 case of RO_2 radicals. By varying the [NO] and knowing the RO_2 --> OH kinetics can identify where RO_2 is
1035 being detected, under these conditions defining HO_2 yields becomes complex as is described in (Nehr et al.
1036 PCCP 2011).

1037 (**Line 355**)

1038 'For test reagents which can generate radicals similar to hydroxyethylperoxy, our instrument will detect
1039 both HO_2 and RO_2 with some selectivity to HO_2. Potential RO_2 interference can be tested by examining
1040 the 'HO_2' yield as a function of added [NO].'

1041

1042 **Comment 9:**

1043 *P15 L357: Could the authors give numbers of the timescales? What fraction of HO2 from R10 would be*
1044 *still seen?*

1045 "the α abstraction still leads to prompt formation of HO2 via R9, but R10, CH3O + O2, occurs on a much
1046 longer timescale"

1047 **Response:**

1048 R9 had a formation rate of over 50,000 s^{-1} compared with R10, which had a formation rate of approximately
1049 10 s^{-1}. Even for the slowest OH and methanol reactions carried out the yield was assigned before 5
1050 millisecond, under these conditions less than 10 percent of this channel, will have formed HO_2 under the
1051 measured timescale. With the HO_2 peak being retrieved from the biexponential fit, it is likely that this
1052 contribution would have been lower than at under 3 percent of this channel being titrated to HO_2 at the point
1053 at which the peak HO_2 signal was observed.

1054 The relevant rate coefficients are presented in **line 366**.

1055 **Comment 10:**

1056 *P15 L370: I kindly disagree with this statement. The yield is the difference between the HO2 yields from*
1057 *both experiments has a large error. The value is (10+/-11)% applying error propagation. What would be*

the additional uncertainty due to potential RO2 interferences and the fraction of HO2 from R10 (see comment above)?

"It has additionally been demonstrated that the instrument had sufficient accuracy and precision to assign the branching ratios for differing abstraction channels when it was possible to separate the channels by the timescale for HO2 generation."

Response:

This statement was based purely on the result of simple statistical significance at the 95 % confidence level. When a Welch's t test (*Biometrika*, 1947) was performed on the low and high oxygen measurements ((0.87 ± 0.10), (0.97 ± 0.06), 2 sigma errors) a t value of 3.41 was derived with 5.10 degrees of freedom, for a 2 tailed test this gave a p value of 0.0184 which is statistically significant at the 98 % confidence level, this result was not significant at the 99 % level.

Further experiments were carried out on this reaction with respect to the question posed by Reviewer 1, and through this work the upper yield has now been revised to 99 ± 4 % where the error is again given as 2 sigma.

When the new revised value for the high oxygen measurements is used the p value returned is 0.0156, again significant at the 98 % level but not the 99 % level.

In the low oxygen experiments the $[O_2] < 1E15$ cm^{-3} and therefore $CH_3O + O_2 < 20$ s^{-1}. When the HO_2 was assigned < 5% of CH_3O would have been titrated to HO_2.

(**Line 375**)

'The resulting observed yield (second row of Table 1) is consistent with 100% conversion of OH to HO_2 and is statistically different from the low oxygen measurements based on a Welch t-test at the 95% level.'

Comment 11:

P16 Section 3.3: The description would benefit from a discussion about the reproducibility of these effects and their impact on the accuracy of results for experiments.

"3.3 Assessment of transport effects on observed kinetics"

Response:

Kinetics measured in the jet require no corrections.

Any kinetics measured in a FAGE expansion outside of the jet itself are subject to transport. The kinetics measured on the second detector are always slower (10% under 250 s^{-1} 50 % at 2500 s^{-1}), this deviation can be corrected for via Figures 6 and 7. The effect of transport on kinetics has been discussed in detail by Stone et al. (R.S.I 2016) and by Taatjes (Int. J. Chem. Kinet. 2007) for transport in the jetting gas. The effects on transport when sampling from high to low pressures is also described in detail in Baeza-Romero et al. (Int. J. Chem. Kinet. 2011), references to these works are included in the provisional revised manuscript (line ***).

Comment 12:

Figure 6/7: The authors should make clear, which experiments are shown in these figures.

Response:

These experiments were measurements of OH and H_2O_2 over varied H_2O_2 concentrations. Legends have now been included, and the description has been updated to provide the experimental detail.

Comment 13:

Table 3: The table is not correctly displayed.

Response:

Thank you, the table will display fine in a final print, the issue is line numbers have displayed over the table as oppose to at the side of the page as would normally be expected. The table itself seems correct though.

Comment 14:

The authors might somewhere discuss the approach used in Nehr et al., PCCP, 2002 to determine HO2 yields.

Response:

Nehr et al PCCP 2011, Phys. Chem. Chem. Phys., 2011, 13, 10699–10708 on HO2 from OH and benzene using a modified OH reactivity instrument does include an interesting and thorough description of assigning HO_2 yields from OH initiated reactions. A discussion of the technique of Nehr et al. and a comparison to the method used in this work will be included.

Material has been added in **lines 126-8**

'The instrument has some similarities to that presented by Nehr et al. (2011) where a conventional OH lifetime instrument was altered to allow for chemical conversion of HO_2 to OH and hence the sequential determination of OH and HO_2.'

and **616-629.**

'As mentioned in the introduction, the instrument has similarities to that presented by Nehr et al. (2011), where a FAGE system for sequential OH and HO_2 is coupled to a lifetime instrument and yields of HO_2 from OH initiated reactions are reported. Although the principles of HOx detection used in both systems is similar, there are some significant differences between the two instruments. Some differences relate to the reaction cell in which the kinetics takes place: 1 atm of air and 298 K for Nehr et al. and 0.5 – 5 atm of any gas and 298 – 800 K for this work. However, in principle, the Nehr et al. FAGE cell could be coupled to a different reaction cell to probe a wider range of conditions. A more substantial difference is the timescale of the chemistry taking place. Typical temporal profiles from Nehr et al. are of the order of a second compared to <10 ms in this work. The enhanced sensitivity of the Nehr et al. instrument means that radical-radical reactions should

not interfere, but the technique may be subject to interferences from first order (or pseudo-first order) reactions including heterogeneous processes. Detection of radicals in kinetics or yield experiments is difficult and studying reactions under a range of conditions is important to identify systematic errors, hence both instruments have a role to play.'

Comment 15:

General remark to the figures: It would be easier to work with legends instead of descriptions in the captions.

Response:

Use of appropriate legends supported by detailed figure captions will indeed improve the overall readability of this work. See above comment.